Application of copper slag in geomagnetic archaeointensity research

E. Ben-Yosef,[1,4] H. Ron,[1] L. Tauxe,[2] A. Agnon,[1] A. Genevey,[3] T. E. Levy,[4] U. Avner,[5] and M. Najjar[6]

[1] Paleointensity and archaeointensity studies since the 1950s have produced numerous geomagnetic intensity data for the last seven millennia. As a consequence of different experiments and materials, there is a complex and internally inconsistent picture of the geomagnetic field behavior. In this study we present data using a recently developed experimental design on a heretofore unexploited recording medium: copper slag deposits. Our results, based on hundreds of specimens from various archaeometallurgical sites of the Southern Levant, demonstrate the applicability of copper slag material for archaeointensity studies. In addition to frequently exhibiting good experimental behavior, slag has further advantages such as dense multilayer deposits and in cases embedded charcoals, which open the door to data sets with excellent age control and resolution. The data presented here augment the high quality database from the Middle East and support previously observed periods of rapid change of the intensity of the geomagnetic field.

Citation: Ben-Yosef, E., H. Ron, L. Tauxe, A. Agnon, A. Genevey, T. E. Levy, U. Avner, and M. Najjar (2008), Application of copper slag in geomagnetic archaeointensity research, *J. Geophys. Res.*, *113*, B08101, doi:10.1029/2007JB005235.

1. Introduction

[2] Enormous effort over many decades has produced a huge amount of data for the ancient geomagnetic field. These data have been incorporated into increasingly sophisticated models. The GUFM model of *Jackson et al.* [2000] allows the interpolation of geomagnetic field vectors as a function of time and location for the last 400 years based on human measurements. *Korte et al.* [2005] and *Korte and Constable* [2005a, 2005b] have extended the analysis to the past 7 ka by using records of lava flows, sediments and archaeological materials in the CALSK7.2 model.

[3] The behavior of the geomagnetic field over the Holocene is of interest to a wide variety of investigators including geophysicists, archaeologists, historians, and paleoclimate researchers. The geomagnetic field is one of the primary controls of radiocarbon production hence strongly affects the radiocarbon calibration curves [e.g., *Peristykh and Damon*, 2003]. Sorting out field variations is key to interpretations of past solar activity [e.g., *Usoskin et al.*, 2006]. An accurate model of geomagnetic field variations of the sort being assembled by for example *Korte and Constable* [2005a] could ultimately provide the long awaited timescale based on secular variation. There has been a recent revival of interest in possible connections between geomagnetic field behavior and climate [e.g., *Yamazaki and Oda*, 2002]. In addition, the geomagnetic field has significantly reduced in strength over the last few decades, leading to speculation that it could collapse entirely as it undergoes a reversal of polarity [*Hulot et al.*, 2002]. The decay in field strength appears to have begun more than 160 years ago [*Bloxham*, 2003] yet prior the mid 1800s there are no actual measurements of field strength. Study of this problem must rely on "accidental records" such as those retained in rocks or fired archaeological materials.

[4] Analysis of the time evolution of the geomagnetic field requires full vector information. The directional variability has been studied extensively by paleomagnetists, and is easier to retrieve than the intensity of the ancient magnetic field. The time of recording (age of rocks or archaeological artifacts) is also usually hard to achieve in high precision. In fact, ancient geomagnetic field intensity is perhaps the most difficult observable to determine using paleomagnetic techniques [see, e.g., *Valet*, 2003]. While a thermal remanent magnetization (TRM) can retain an excellent record of the geomagnetic direction, recovery of the intensity requires arduous laboratory experiments, the interpretation of which can be controversial. The assumptions behind the method demand that the experimental material retains a primary magnetization of thermal origin and also behaves "well" during the paleointensity experiment. Crucial requirements are that the material (geological or archaeological) not alter during the experiment and that the temperature at which the material becomes magnetized (the blocking temperature) is the same as that at which it becomes demagnetized (or remagnetized) (the unblocking temperature). The optimal

[1]Institute of Earth Sciences, The Hebrew University of Jerusalem, Jerusalem, Israel.
[2]Scripps Institution of Oceanography, University of California, San Diego, La Jolla, California, USA.
[3]Centre de Recherche et de Restauration des Musées de France, Palais du Louvre, Paris, France.
[4]Department of Anthropology, University of California, San Diego, La Jolla, California, USA.
[5]The Arava Institute for Environmental Studies, Kibbutz Ketura, M. P. Hevel Eilot, Israel.
[6]Department of Antiquity, Amman, Jordan.

experimental design builds in tests for these assumptions so that spurious data can be identified and rejected.

[5] Even if the intensity can be measured with high confidence, it is of little value without a rather precise knowledge of the sample's age. Volcanic rocks are frequently used for absolute paleointensity measurements. They can meet the requirements for paleointensity analysis, and in addition can often be dated by radiometric methods. The accuracy depends on the method chosen for a given age span. Age determination of young (<50 ka) lava flows, the target of many paleointensity studies, frequently depends on the association of rare organic materials trapped in or under the rock. Sediments can also be used for study of the ancient geomagnetic field [see, e.g., *Tauxe and Yamazaki*, 2007], but paleointensity information is at best relative and the timescales are sometimes difficult to constrain. Because archaeological materials can often be dated by radiocarbon or by cultural context they have long been attractive targets for studies of the ancient magnetic field [see, e.g., *Folgheraiter*, 1899; *Thellier*, 1938].

[6] The symbiosis of archaeology and archaeomagnetism has a long and distinguished record. The study of the ancient geomagnetic field requires materials that retain a record of the magnetic field vector that can be retrieved in the laboratory. On the other hand, archaeomagnetic studies might be of benefit to archaeological studies. Comparison of the magnetic vector with previously established variations of the magnetic field can provide age constraints on poorly dated archaeological material. Yet prior efforts in archaeomagnetism have been hampered by the difficulty in obtaining the strength of the vector owing to the lack of suitable material and/or poor age control. As a result, many regional data sets are highly scattered during certain time intervals, hindering the development of geomagnetic field models that would enable interpolation of geomagnetic field vectors with high reliability.

2. Middle East Paleointensity Records

[7] As one of the hearth areas for the beginnings of sedentism, the emergence of agriculture, and the rise of social complexity, the Middle East has a wealth of archaeological sites. Archaeological remains that are suitable for archaeomagnetic investigation first appear in the region some 10,500 years ago, during the "Neolithic revolution" [e.g., *Simmons*, 2007]. During this period humankind first invented pyrotechnological products such as ceramics, in addition to the first use of mud bricks in sedentized settlements. Archaeological fired clay has been the primary material for archaeomagnetic investigation.

[8] Paleointensity variations in the Middle Easter over the last seven millennia (see Figure 1 and caption) have been the focus of intensive studies. As summarized by *Genevey et al.* [2003], different records over the past five millennia from Syria, Central Asia and Bulgaria agree quite well, while those from about 7000 to 5000 years ago do not. Geomagnetic field intensity estimates obtained from Syrian bricks and pottery samples from between 6000 and 7000years ago are about 70% of the present field intensity [*Genevey et al.*, 2003; *Gallet and Le Goff*, 2006], while records from Bulgaria, Georgia and Central Asia show values up to and exceeding the present geomagnetic field

intensity [*Kovacheva et al.*, 1998; *Burakov and Nachasova*, 1988; *Nachasova and Burakov*, 2000]. Differences in experimental design, data selection criteria, or genuine spatial variability in the ancient geomagnetic field are possible explanations for the discrepancies and new data are required to solve this problem.

[9] The data from Syria of *Genevey et al.* [2003], *Gallet and Le Goff* [2006], and *Gallet et al.* [2006] are the best archaeological paleointensity data from the region. They are well dated and mutually consistent. The data of *Gallet and Le Goff* [2006] and *Gallet et al.* [2006] were not included in the CALS7K.2 model, so they serve as a test of its predictive capability. We show the model predictions for Syria as a dashed line in Figure 1. The CALS7K.2 model has a variable degree of success in predicting paleointensities from Syria. There are times during which the CALS7K.2 predictions underestimate the Syrian data by some 10%. This is likely due to the high degree of scatter in the published data during these time intervals and the limited resolution of the model, as pointed out by *Korte et al.* [2005] and in more detail by *Korte and Constable* [2006]. It seems that more, well dated and experimentally reliable data would be helpful in improving the CALS7K type models.

3. Archaeometallurgy in the Southern Levant

[10] To overcome the main two difficulties of suitability for the paleointensity experiment and age resolution of archaeological materials, we have begun systematic investigations of archaeological copper smelting slag deposits. Slag deposits, formed by fast cooling melts derived from silicate and carbonate copper ores, may be nearly ideal for paleointensity study. Many slag samples have portions that are very fine grained. Many specimens have magnetic particles that are extremely small, spanning the size range that is most desirable for the intensity experiment. In some cases slag can be collected as oriented or at least partially oriented (horizontal) samples, allowing directional analysis as well. Frequently, slag traps charcoal fragments from the smelting furnace which would enable radiometric dating by [14]C. Hence slag has the possibility of combining the advantages of good performance during the paleointensity experiment and the availability of precise radiometric dates. In many localities slag deposits are found as large multilayer waste mounds which represent intensive copper production in certain periods (Figure 2). Profiles of such mounds could be an invaluable high resolution recording of the geomagnetic field intensity in these periods.

[11] The copper ore rich district of southern Israel and Jordan is one of the most comprehensive regions for mining and metal production sites spanning the Chalcolithic (ca 4500 BCE) through Islamic periods (ca 1516 CE). Slags from the Levant provide an exciting new sample set for refining the archaeointensity curve. In turn, intensity data could be used to help sort out controversies regarding ages of material obtained prior to modern, sophisticated excavations (i.e., samples of the same age should have the same intensity).

[12] The first evidence of copper production in the Southern Levant goes back as early as the 5th millennium BCE and corresponds with the period of metallurgical
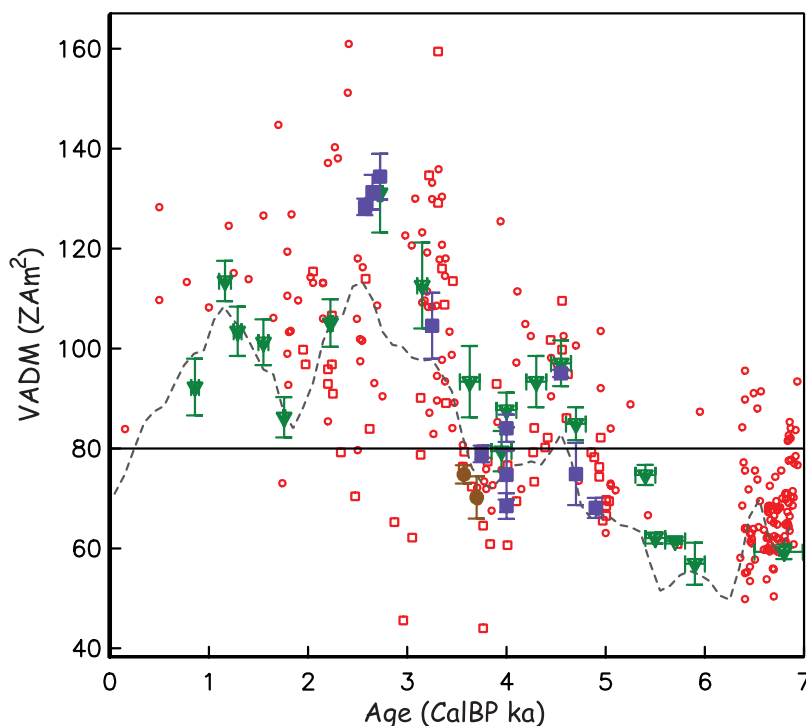
Figure 1. Summary of available archaeointensity data from the Near and Middle East for the last seven millennia, the period since the inception of copper smelting. The magnetic intensity is expressed as Virtual Axial Dipole Moment [$Z = 10^{21}$]. Large green triangles are data from Syria of *Genevey et al.* [2003], blue squares are from *Gallet and Le Goff* [2006] and brown dots are the Syrian data from *Gallet et al.* [2006]. Open circles are data from thermally blocked remanences from the Near East of *Aitken et al.* [1984]; *Athavale* [1969]; *Hussain* [1983, 1987]; *Odah et al.* [1995]; *Odah* [1999]; *Nachasova and Burakov* [1995]; *Walton* [1977, 1986, 1990]. The small open squares are data of *Games*, [1980] that are largely from adobe bricks (not a thermal remanence). Predicted VADM values for Syria by CALS7K.2 of *Korte and Constable* [2005a] are shown as dashed line. The present field value is shown as a solid black line ($\sim$80 ZAm^2).

innovation throughout the ancient Near East [e.g., *Avner*, 2002; *Rothenberg*, 1990; *Hauptmann*, 1989; *Levy and Shalev*, 1989]. For the first time humankind learned to produce metallic copper from ore, an elaborate process that signifies a notable change in the archaeological records. The art of smelting requires pyrotechnological skills such as furnace construction to achieve temperatures above 1100°C. The basic technique involved preparation of the smelting mixture (copper ores and other minerals which are used as fluxes), charcoal manufacture and construction of high-temperature furnaces. These probably made use of a bellows system including tuyères and/or bellows pipes from the beginning.

[13] Beyond the basic elements, the techniques used for making copper vary in different regions and different times. There were significant developments in certain archaeological periods such as the use of wind-powered furnaces during the third millennium BCE or large scale industrial production in the first millennium BCE [e.g., *Hauptmann*, 2000].

[14] The most dominant remnants of copper production activities are deposits of slag, the solidified residue of melted material that remains after the extraction of copper from the mixture of ores and fluxes. Slag pieces can be found in different quantities and sizes in almost every

archaeological site where copper production occurred, from small scale workshops to ancient industrial scale production.

[15] The Southern Levant has an abundance of archaeometallurgical sites. These are concentrated mainly along the two sides of the 'Arava valley (Wadi Arabah) which straddles the southern border of the modern states Jordan and Israel (Figure 3). The largest center of copper production in the eastern Mediterranean (excluding Cyprus) is the region of Faynan in the northern 'Arava valley [e.g., *Hauptmann*, 2000; *Levy et al.*, 2001, 2002, 2004; *Hauptmann and Weisberger*, 1987, 1992]. It contains slag deposits spanning the last six millennia that were initially studied by the German Mining Museum [*Hauptmann*, 2000] and most recently are the focus of intensive archaeometallurgical investigation as part of the University of California in San Diego/Department of Antiquity of Jordan Edom Lowland Regional Archaeology Project [e.g., *Levy*, 2006]. Further south in the 'Arava valley, a smaller copper production center is located in the region of Timna in Israel. Its slag deposits, probably spanning the last 6500 years, were investigated for more than 40 years by the 'Arava archaeological expedition [e.g., *Rothenberg*, 1999, 1990]. Intermittent archaeological research in Timna continues to today.

Figure 2. Sampling profile of large slag mound at Khirbat al-Jariya, Jordan. The accumulation of multilayer slag waste has the potential for high resolution archaeointensity investigation in certain periods.

[16] Beyond these two large-scale copper production centers mentioned above, there are additional sites with copper industry remains in other parts of the Southern Levant such as the southern Sinai Peninsula [*Bachmann*, 1980; *Rothenberg*, 1987] providing a continuous sequence of slag deposits spanning the past 5500 years. The great abundance of slag remains in archaeometallurgical sites enables us to create a collection of slag samples with a large range of ages, locations and types.

4. Slag Material

[17] Slag samples vary in chemical composition, appearance, size, mineralogy and texture depending on the original ore and flux mixture and the specific technique of smelting used. In the Southern Levant, where the copper ores originate mostly in sandstone host rocks [*Schlomovitz et al.*, 1999], slag is usually composed of two major mineral groups: silicates and iron oxides. Each mineral group comprises between 10–40% of the slag weight (Table 1). In some cases, the dominance of iron oxides can be replaced by other minerals depending on the different types of fluxes used. For example in Faynan, owing to the high manganese concentration in the ore, no additional iron flux was added

during smelting. The resulting slag is therefore lower in iron and higher in manganese [e.g., *Hauptmann*, 2000] (Table 1).

[18] Copper production technologies and slag typology are subjects of active research. In this study we applied a crude typology based on available studies from the Wadi 'Arabah research area [*Hauptmann*, 2000; *Rothenberg*, 1990]. Our typology derives from the two main technologies that produced different types of slag (here called informally "furnace slag" and "tapping slag"), which have easily distinguishable visual differences.

[19] The earliest technology, which produced furnace slag, used pit furnaces (see example in Figure 4a) into which ore and flux were introduced with or without a crucible. The smelting process resulted with incompletely smelted ores, that were part of relatively inhomogenous slag. The slag was usually taken from the furnace and crushed (see Figure 4b) to extract the copper prills. Sometimes they were remelted to further extract copper. The furnace slag procedure was developed in the Chalcolithic (ca 4500–3600 BCE) and was common until the Early Bronze Age II (ca 3000–2000 BCE) when it was replaced by the "tapping technology".
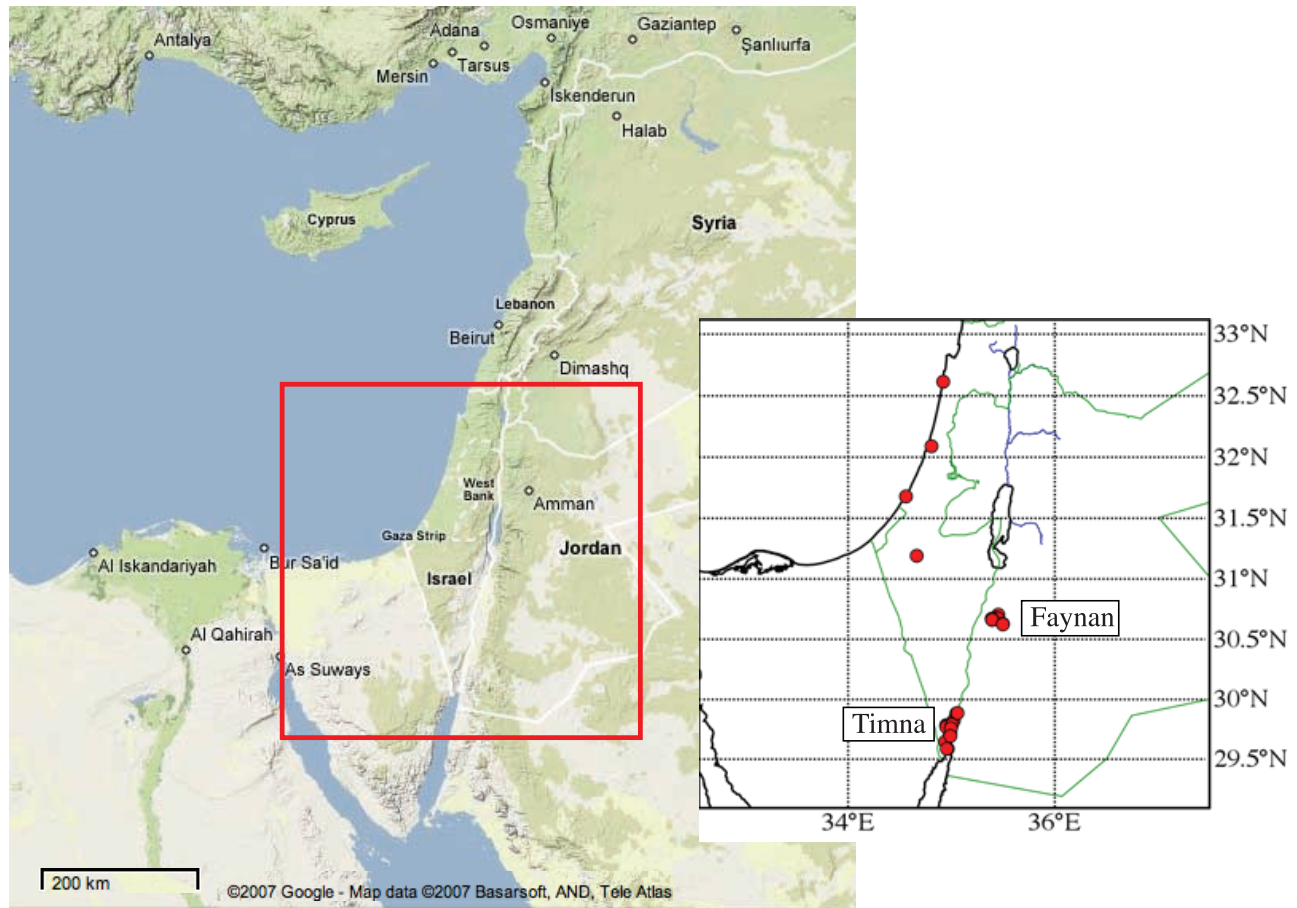
Figure 3. Map showing the locations of sampling sites from Table 2 (red dots). Also shown are Timna and Faynan, the two main areas of copper production in the Southern Levant.

[20] Tapping slag is the result of a complicated smelting process aimed at achieving complete separation between slag and metallic copper. In this technique the heaviest part of the melted mixture sinks to the bottom of the furnace and solidifies in the form of a copper chunk. The lighter material was tapped off and allowed to pour out of the installation. This tapping slag cools on the ground and frequently has observable flow textures (Figures 4c and 4d) and can be

Table 1. Examples of Mangenese, Iron, Silica and Copper Content (by % Weight) of Copper Slag From Representative Locations

Ref.[a]	Phase[b] Analysis (XRD)	MnO %	FeO %	SiO$_2$ %	Cu %	Samp. ID	Loc.[c]	Arch. Period[d]
				FS				
1	-	-	21.69	34.25	15.12	58a	Timna 39b	Chal.
1	Del, Fay, Q, Sp	2	49.51	30.71	1.3	50	Timna 39b	Chal.
2	Q, Del	0.02	12.1	38,8	21.5	284-2235-2	ASH	EB I
2	Fay, Mag, Cup	0.01	45.1	10.2	9.4	284-2262	ASH	EB I
				TS				
5	-	2.7	32.9	35.7	2.3	LR5	Timna 2	LBII-IrAI
5	-	3.5	40.4	36.1	0.32	LR7	Timna 2	LBII-IrAI
3	Teph, Glass	40.7	3.9	32.7	0.37	2/5A	KEN	Iron Age
3	Teph, Glass	37.5	3.61	32.1	0.4	2/2B	KEN	Iron Age
				ATS				
3	Bust, Teph, Glass	32.9	5.26	42.6	0.56	1/23A	Fenan 1	Roman
4	-	1.74	27.9	38.63	0.99	127B	Timna 28	Early Islamic
4	Sp, Hed	2.03	37.83	24.73	1.28	134	Timna 28	Early Islamic
3	Kneb, Px, Glass	14.3	38.4	34	1.33	6/2A	El Furn	Mamluk

Slag types: ATS = Advanced Tapping Slag, FS = Furnace Slag, TS = Tapping Slag.
[a]References: [1] *Lupu* [1970], [2] *Segal et al.* [2004], [3] *Hauptmann and Weisberger* [1987], [4] *Rothenberg* [1990], [5] *Lupu and Rothenberg* [1980].
[b]Phases: Bust = Bustamite, (Mn,Ca)3Si3O9, Chal. = Chalcolithic, Cup-Cuprite, Cu$_2$O, Del = Delafossite CuFeO$_2$, Fay = Fayalite, Fe$_2$SiO$_4$, Hed = Hedenbergite, CaFeSi$_2$O$_6$ (Pyroxene), Kneb = Knebelite, Fe$_2$SiO$_4$, Mag = Magnetite, Fe$_3$O$_4$, P = Pyroxene, Q = Quartz, Sp = Spinel, Teph = Tephroite, Mn$_2$SiO$_4$.
[c]Localities: ASH = Ashqelon-Afridar, KEN = Khirbat en Nahas.
[d]Archaeological Periods: EBI = Early Bronze I, IrAI = Iron Age I.

Figure 4. Examples of different sample types. (a) Intact furnace with in situ slag attached to the clay wall (Furnace Z at Timna 2, Late Bronze Age-Early Iron Age, Israel). Scale approximately 15 cm. (b) Broken furnace slag pieces (from the site of Timna 39b, Israel). (c) Broken tapping slag plate with flow texture (Tell Hara Hadid, Early Islamic period, Israel). (d) Complete tapping slag with flow texture (Khirbat Hamra Ifdan, Faynan, Jordan). (e) and (f) glassy fragments of tapping slag (Khirbat en-Nahas, Iron Age, Jordan). (g) "Slag cake" (Beer-Ora valley, Early Islamic period, Israel). (h) Fragment of clay crucible with thick slag glaze (Tell Garisa, Early Iron Age, Israel). (i) Rod clay and fragments of clay linings of a wind operated furnace (site of Fenan 15, Early Bronze Age II-3, Jordan).

very glassy (Figures 4e and 4f). Tapping technology evolved considerably through time culminating in the Islamic Period (640–1099 CE) with the introduction of huge slag rings (Figure 4g). These were made by pouring the melt into a prebuilt depression and enabled the fast removal of the production waste (i.e., slag) and the continuous operation of the smelting installation, thus producing a large amount of copper.

[21] It is likely that tapping slag cools to ambient temperature very quickly (within less than an hour) and furnace slag cools more slowly, but is cool to the touch within a few hours. In many cases, slag has a glassy texture with iron oxide and metal phenocrysts. Although tapping slag tends to be glassier than furnace slag, glass is still observed in furnace slag.

[22] The ring in the tapping slag cake was made to allow the slag makers to move the slag cake around while it is still too hot to touch. It is therefore possible, if not likely, that such slag will have multicomponent remanences reflecting the high temperature quenching component followed by lower temperature components acquired as the slag cake is moved about. A similar effect could occur also in furnace slag when the furnace was broken apart while it was still hot.

5. Sample Collection and Age Determination

[23] We collected slag samples from 27 archaeometallurgical sites in Israel and Jordan (Table 2). In addition to furnace and tapping slag, some of the samples are from fired clay related to the copper industry (see examples in Figures 4h and 4i). These are primarily fragments of crucibles and furnace linings that mostly originate from the same context as our slag samples. Other slag samples derive from Bronze production, which together with the fired clay samples enable us to investigate a wider range of

Table 2. Site Locations and Age Constraints

Site	Locality	Type[a]	Latitude	Longitude	C.[b]	Age[c]	Q.[d]	Meth.[e]	Ref.[f]
IS01	Hai-bar	FS	29.830	35.020	S	5350 ± 1100	5	A	1
IS02	Timna 149-hill top	FS	29.792	35.001	S	4100 ± 150	5	A	2,3,5,6
IS03	Timna 149-hillside	FS	29.792	35.001	S	4100 ± 150	2	A	2,3,5,6
IS04	Timna 28	TS	29.716	34.984	S	1100 ± 150	2	C	4,7,9
IS05	Timna 2	TS	29.784	34.948	S	3175 ± 75	2	C:A	10
IS06	Timna 2	TS	29.784	34.948	S	3175 ± 75	2	C:A	10
IS07	Beer Ora Hill	FS	29.717	34.985	S	3735 ± 20	2	C	6
IS08	Timna 3	TS	29.779	34.952	S	3175 ± 75	2	A	5
IS09	Timna 30	TS	29.771	34.947	S	2810 ± 60	3	C:A	10
IS10	Tell Hara Hadid	TS	29.589	34.965	S	1150 ± 150	3	A	1
IS11	Timna 39b	FS	29.762	34.994	S	6150 ± 250	6	A	6,11−13,33
IS14	Shiqmim	FS/C	31.195	34.639	E	6225 ± 50	1	C	14−16
IS15	Yotvata EB	FS	29.885	35.046	S	4600 ± 350	5	A	1
IS16	Yotvata Nabataean	TS	29.885	35.046	S	1950 ± 100	1	A	1
IS17	Yotvata Fortress	FS	29.890	35.058	S	5810 ± 500	3	C	17,8,6
IS18	Givat Yocheved	TS	29.648	34.939	S	1150 ± 150	6	C	9,18,10
IS19	Eilot quarry	FS	29.589	34.952	S	4600 ± 350	5	A	1,20
IS20	Ashkelon-Afridar	FS/C	31.679	34.556	E	5425 ± 125	4	A:C	21−24
IS21	Tell Gerisa	BS	32.091	34.806	E	3050 ± 100	3	A	25
IS22	Tell Dor	BS	32.617	34.916	E	3050 ± 100	1	A	26
IS23	Timna 149-hill top	FS	29.792	35.001	S	4100 ± 150	6	A	2−6
IS24	Timna 39b	FS	29.762	34.994	S	6150 ± 250	6	A	6,11−13,33
IS25	Mitzpe Evrona	TS	29.695	34.987	S	1150 ± 150	3	A	9
JS01	Fidan 4	FS/C	30.673	35.385	S	5200 ± 250	1	C	27,28
JS02	Khirbat al Jariya	TS/C	30.707	35.452	S	2980 ± 110	1	C	28
JS03	Khirbat en Nahas	TS	30.681	35.437	S	2800 ± 50	1	C	29,28,30
JS04	Fenan 15	FS/C	30.629	35.497	S	4550 ± 300	1	A	28
JS05	El-Furn	TS	30.675	35.447	S	700 ± 50	1	A	28
JS06	Khirbat Hamra Ifdan	TS	30.663	35.393	S	2950 ± 200	4	A	31,32
JS07	Wadi Fidan 77a[g]	FS	30.674	35.391	E	2950 ± 200	3	A	32
JS08	Khirbat Hamra Ifdan	FS	30.663	35.393	E	4050 ± 100	1	A:C	31
JS09	Khirbat Hamra Ifdan	FS	30.663	35.393	E	4400 ± 150	1	A:C	31
JS10	Fenan 7	TS	30.630	35.495	S	2850 ± 100	5	A	28
JS11	Fenan 1	TS	30.626	35.495	S	1790 ± 145	2	A:C	28

[a]Type: FS, furnace slag; TS, tapping slag; C, clay; BS, bronze production slag.
[b]Collection method: S, Surface collection during survey; E, Collection from excavation.
[c]All ages are years before 1950.
[d]Age quality: 1, Excellent; 2, Moderate to excellent; 3, Moderate; 4, Moderate to Poor; 5, Poor; 6, Controversial.
[e]Dating Methods: C: [14]C (ages are calibrated BP), A: archaeological context.
[f]Most relevant references: [1] U. Avner, personal communication, 2006, [2] *Rothenberg and Shaw* [1990a], [3] *Rothenberg and Shaw* [1990b], [4] *Rothenberg* [1999], [5] *Rothenberg and Glass* [1992], [6] *Avner* [2002], [7] *Sharon et al.* [1996], [8] *Segal and Carmi* [1996], [9] *Avner and Magness* [1998], [10] *Rothenberg* [1990], [11] *Rothenberg* [1978], [12] *Rothenberg and Shaw* [1990b], [13] *Muhly* [1984], [14] *Gilead* [1994], [15] *Shalev and Northover* [1987], [16] *Burton and Levy* [2001], [17] *Meshel* [1993], [18] *Willis* [1990], [20] *Avner and Naor* [1978], [21] *Segal and Carmi* [2004], [22] *Gophna* [2004], [23] *Golani* [2004], [24] Y. Yekutieli, personal communication, 2006, [25] Z. Herzog, personal communication, 2005, [26] *Ilan* [1999], [27] *Adams* [1999], [28] *Hauptmann* [2000], [29] *Levy et al.* [2004], [30] *Levy et al.* [2005], [31] *Levy et al.* [2002], [32] T. Levy, personal communication, 2007, [33] *Burleigh and Hewson* [1979].
[g]Wadi Fidan 77a is also known as Khirbet Glueck.

materials derived from high-temperature industry as well as to compare among them.

[24] Most of the samples were collected during a field survey from a variety of archaeological contexts. The survey was carried out during the years 2004–2005 under the auspices of TL and MN in Faynan area and UA and A. Holtzer in Timna. Other samples were taken from collections of previous archaeological excavations with the exact locations well known (e.g., the sites of Shiqmim and Khirbat Hamra Ifdan, see Table 2) providing the best reference for further analysis.

[25] The main criteria used for choosing the sites were: (1) dating quality, with priority given to sites that have well established archaeological dating or good results from ^{14}C measurements; (2) sites from periods that have distinct geomagnetic archaeointensity trends in previous studies, such as the conspicuous peak in the Iron Age (ca 3000 years ago) and the low in the Chalcolithic-Early Bronze Age (ca 5500 years ago); and (3) sites in which

archaeointensity data might help solve questions concerning the history of metallurgical technology, such as Timna 39b and Timna 149.

[26] The archaeological context constraining the age information of the slag collection (see Table 2) is of variable quality. We have developed a scheme of qualifying the age of a sample based on the complex reality of archaeological investigation in our research area. At this point, slag samples themselves have not been directly dated with radiocarbon techniques (although that will be done for many samples in the future). Therefore a given age determination depends on both the archaeological context and the reliability of the age assigned to a given locality. The age may be precise, but the archaeological context tying a given sample to a given age may be weak or controversial. In order to qualify the context itself, we make use of various objective categories that relate to the methods of the archaeological investigation. For example, an age can have a small uncertainty, but the tie to a particular piece of slag
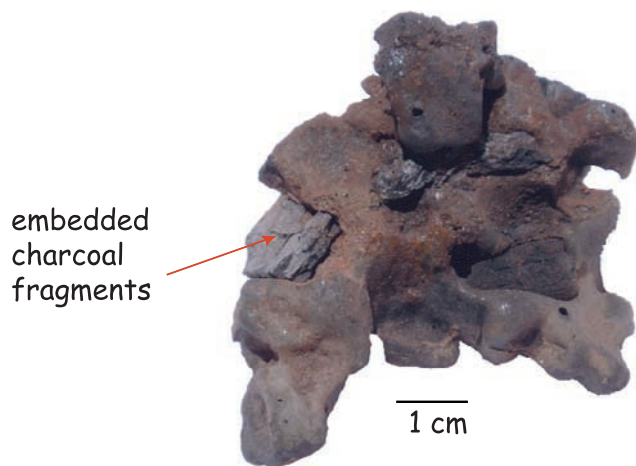
Figure 5. Slag with charcoal embedded in it.

may be unclear because it was collected from the surface (and not from more confined excavated locus) or because the date derives only from an insecure ceramic typology, or other methodological variables. In addition, some of the dates for our slag localities are under scholarly debate, with quite distinct ages being advocated.

[27] To summarize the relative quality of our slag ages, we have assigned each age a number from 1 to 6 where by 1 is considered excellent and 5 is poor. Controversial sites are assigned a number 6. The main criteria for characterizing the age reliability are the archaeological context and the dating technique. We have more confidence in the ages of samples from excavations than surface surveys. Similarly samples that were collected from sites dated with radiocarbon rate better than those dated by ceramic typology alone. For the purposes of geomagnetic field modeling, only those with quality determinations of 1 and 2 should be considered.

[28] Slag has the potential for independent dating without the need of relying on the archaeological context. In many samples, mostly from the more advanced production techniques, we find pieces of charcoal embedded inside the slag which can be used for ^{14}C dating method (Figure 5). We have not yet obtained new dates for the current study.

[29] In this research all of the samples were collected unoriented, enabling us to determine only the intensity of the ancient geomagnetic field. In rare cases we find furnaces in situ (see, e.g., Figure 4a) suggesting the possibility of full vector analysis in future studies. Moreover, tapping slag frequently has quasi-horizontal surfaces which could be used for partially orienting such material.

[30] From each sample (here taken to be a single piece of slag and/or ceramic), we isolated four to twelve specimens ranging from 2 to 7 mm in diameter. Where possible we selected the glassiest material from the outer margins of the slag sample. The specimens were inserted into non-magnetic glass tubes (1 cm in diameter) and fixed into position with silica filter paper and potassium-silicate glue. The tubes were scribed to maintain orientation throughout the archaeointensity experiment. In addition, small chips from the slag specimens (<30 mg) were prepared for hysteresis experiments.

[31] In this study, every coherent fragment (piece of slag or clay) that we collected is called "sample", and every chip of a sample is called "specimen". The full name of a specimen designates its location. JS stands for Jordan, IS stands for Israel and the next two digits represent the site. The sample piece is designated with a letter and the specimen number with the last two digits. For example, specimen JS01b03 is the third specimen from the b sample from the Wadi Fidan 4 site in Jordan. We catalogued and stored all of our samples in the paleomagnetic laboratory of the Institute of Earth Sciences in the Hebrew University of Jerusalem, and they constitute a large inventory for future research.

## 6. Magnetic and SEM Characterization of the Samples

[32] Hysteresis behavior was determined for representative slag specimens (Figures 6 and 7). Hysteresis loops (see insets to Figure 6) were analyzed as follows. First the high field slope (χ_{hf}) was subtracted from the loop. The statistics of interest here are the saturation magnetization (the saturation value of the slope corrected loop, or M_s), the saturation remanence (the y-intercept, or M_r) and the coercivity (x intercept or B_c). The ascending curve was subtracted from the descending curve to calculate the so-called "ΔM curve". The field at which the ΔM curve is 50% of the initial value is the coercivity of remanence B_{cr} [see, e.g., *Tauxe and Yamazaki*, 2007]. We plot the ratio of saturation remanence to saturation versus the coercivity in Figure 7a and versus the ratio of coercivity to coercivity of remanence in Figure 7b. These plots suggest that magnetic grain size of the slag material ranges from single domain ($M_r/M_s > 0.5$) to multidomain ($M_r/M_s < 0.05$).

[33] As part of the paleointensity experiment described in the following, we obtain blocking temperature spectra for all the specimens. These are highly correlated with the type of ore used in smelting. As noted before, some slag samples have high iron concentrations relative to manganese whereas others (typically from the Faynan region) have lower iron and higher manganese concentrations. Figure 8a shows the blocking temperature spectra from typical iron-rich specimens. These are quite common in the slag from Israel. Figures 8b and 8c show blocking temperature spectra from typical manganese-rich specimens common in the Jordanian slag. The iron-rich slag has blocking temperatures characteristic of magnetite (maximum of around 580°C), whereas the manganese rich slag has lower blocking temperatures ranging from around 300 to 450°C (Figures 8b and 8c) typical of copper-manganese ferrites [*Rezlescu and Cuciureanu*, 1970] observed in Faynan [*Hauptmann*, 2000].

[34] We have analyzed representative furnace and tapping slag samples using petrographic and scanning electron microscopes. We detected large scale textures and in cases some mineralogical character using the simple petrographic light microscope, but detailed analysis of the chemical composition, representative mineralogy and textures was achieved by using SEM. In addition to copper, iron and silica minerals, we observed native copper prills in various sizes (Figure 9). Even in the case of tapping slag, only a small portion of the sample has a glassy texture (see enlargement in Figure 9), nevertheless, these "pockets" of
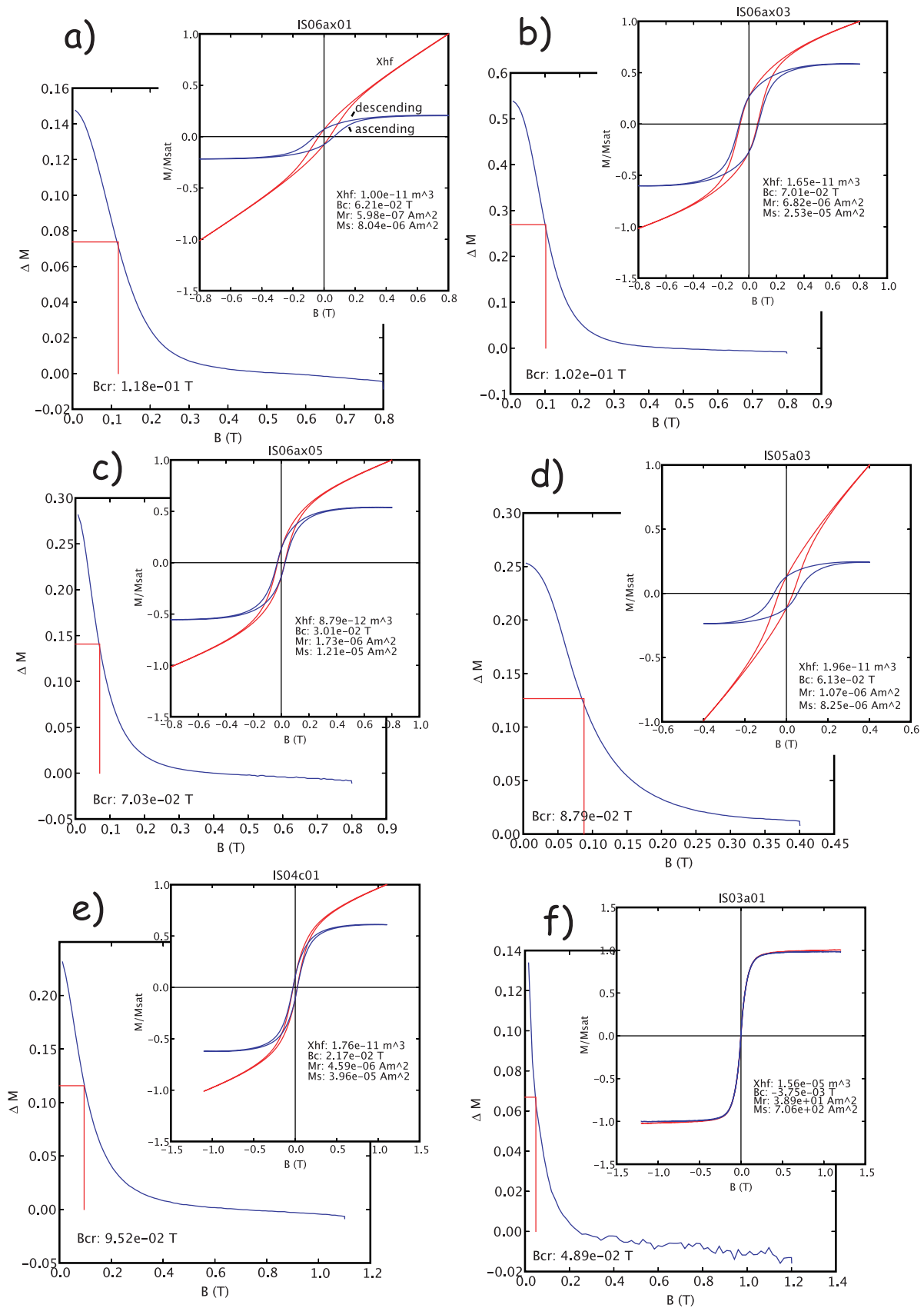
Figure 6. Representative hysteresis loops. The behavior ranges from nearly ideal single domain (a and b) to multidomain (f).
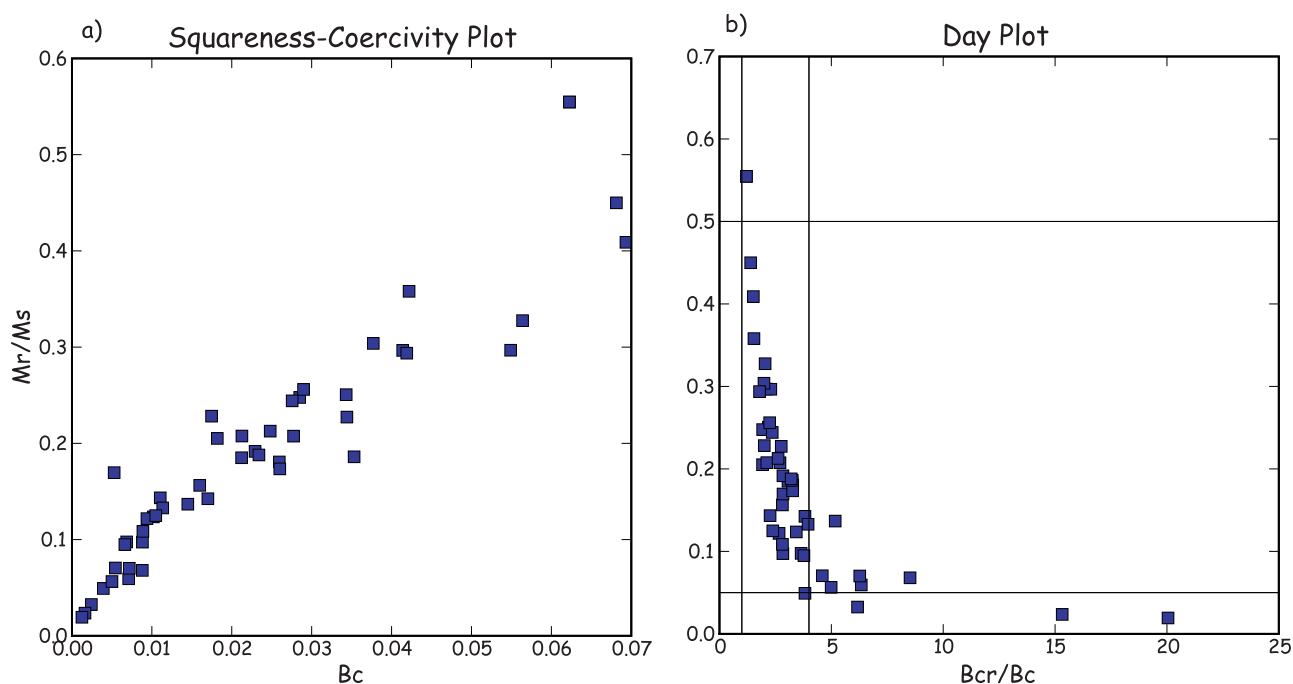
Figure 7. (a) Plot of M_r/M_s against coercivity. (b) Plot of the same against B_{cr}/B_c.

glassy material appear also in furnace slag. Some general examples of common mineralogical phases of slag are presented in Table 1.

[35] Slides made from a cross section of tapping slag reveal clear flow textures expressed also in the mineralogical crystallography (Figure 10). The advanced technology that produced tapping slag involves pouring the molten material out of the furnace and the material probably cooled during flow. As mentioned above, these flow textures are visible also at the sample level (Figures 4c and 4d). The flow texture could have a direct influence on the anisotropic characteristic of tapping slag samples as was observed for

other material with "enforced" textures (i.e., ceramics [*Aitken et al.*, 1981]).

7. Controlled Remelting of Slag Material

[36] To investigate the potential for slag material to retain a record of the magnetic field in which they were formed, we remelted two slag samples under controlled conditions and a known magnetic field intensity. One sample (IS12a) was originally a furnace slag from an ancient technology (Yotvata Fortress) and the second (IS13a) was originally a tapping slag from an advanced technology (Yotvata-Nabataean). We crushed the samples into fragments of
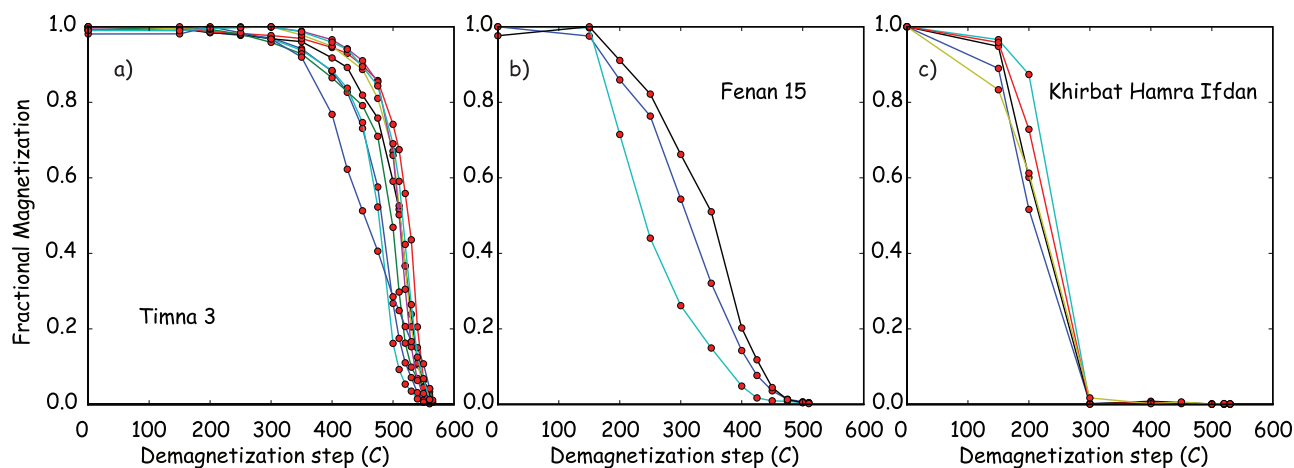
Figure 8. Blocking temperature spectra of typical slag samples. (a) Iron-rich sample (IS08) from Timna 3, Israel. (b) Manganese-rich ore sample (JS04) from Fenan 15, Jordan. (c) Manganese-rich ore sample (JS06, JS08, JS09).
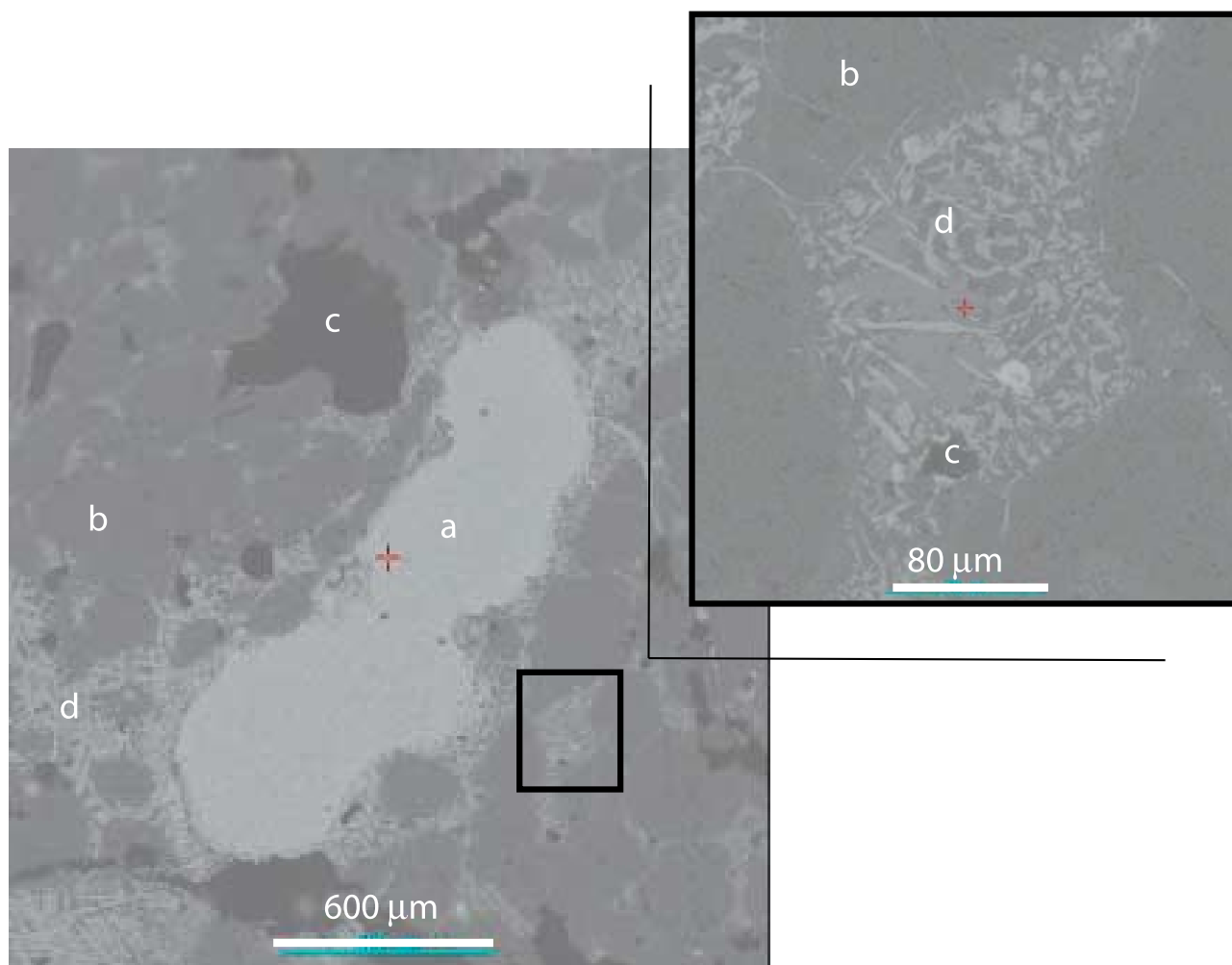
Figure 9. Backscattered image of slag sample from Timna 149, Israel (Electron probe micrograph). The sample contains (a) copper prills, (b) SiO_2 grains (mostly quartz), (c) glassy matrix and (d) copper and iron oxidized minerals.

few centimeters and placed them in ceramic crucibles. We used a high temperatures furnace (Model 88-D, AMKinls) for heating the samples. Melting was done in two stages. In the first stage we used 1200°C for 50 min, and in the second stage we used 1300°C trying to achieve full melting of the slag. After 40 min the tapping slag sample was completely remelted. We took it out with a tong and placed it in a designated location in which the intensity of the magnetic field was measured with three-axis fluxgate magnetometer (35.8−36 μT). After about 15 min the sample was solid again, and it had cooled to below the Curie temperature. We continued to heat the furnace slag sample for additional 30 min, and although it was still only partially molten we took it out and placed it to cool in the same designated location with known magnetic field intensity. We prepared three specimens from each sample for the "paleointensity" experiment described in the next section.

8. Paleointensity Experiment

8.1. Basic Concepts

[37] Paleointensity experiments rely on the fundamental observation that in low fields like the geomagnetic field,

thermal remnant magnetization (TRM) is approximately linearly related to the field in which the material cools. While this is not true for highly elongated magnetic particles [see *Selkin et al.*, 2007], it is likely to be true for the roughly equant magnetic particles characteristic of slag.

[38] In Thellier-Thellier type experiments [*Thellier and Thellier*, 1959], we replace the natural remanence (NRM) progressively with a laboratory TRM. The NRM/TRM ratio multiplied by the laboratory field gives the estimation of the ancient geomagnetic field. We heat the specimens in stages, at least twice to each successive temperature step. This progressive approach allows the detection of nonideal behavior that would violate the assumptions in the technique and lead to unreliable paleofield estimates.

[39] There are two commonly used protocols for the Thellier-Thellier experiment. In the zero-field, in-field'' (ZI) experiment [e.g., *Coe*, 1967] specimens are heated first to a given temperature T_1 (Figure 11) and cooled in zero field. The portion of the NRM with blocking temperatures (T_b) below T_1 will be demagnetized (shown as white). Then the specimen is heated again to T_1 and cooled in a laboratory field B_{lab}, acquiring a partial thermal remanence (pTRM) with a maximum blocking temperature of T_1
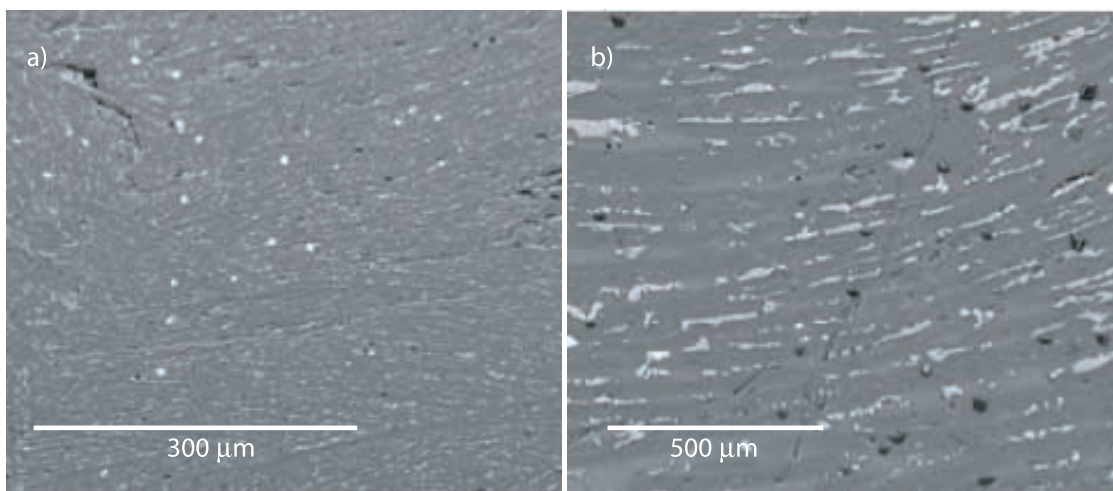
Figure 10. (a) Flow texture in tapping slag sample from Timna 28 (SEM). (b) Same sample in different magnifications.

(shown as grey). Often, (for example after the temperature step labeled T_3) an intermediate step is also performed whereby the specimen is heated to some lower temperature (e.g., T_1 in Figure 11) and cooled in B_{lab} remagnetizing that portion of the remanence with unblocking temperatures below T_1. This is done to check if the partial thermal remanence (pTRM) acquired in T_1 is the same as that acquired initially. This step is known as the "pTRM check" step and is helpful in detecting changes in the capacity of the specimen to acquire TRM caused by alteration during the experiment. Such changes lead to bias in the resulting NRM-TRM relationship and unreliable paleointensity estimates.

[40] Following an in-field step (for example at T_3 in Figure 11), the specimen can be heated again to T_3 and cooled in zero field. This step, the so-called "pTRM tail check" step of *Riisager and Riisager* [2001], can detect if the pTRM acquired at T_3 is completely erased by reheating to T_3. In other words, it tests whether the maximum block-ing temperature of the pTRM is equal to the maximum unblocking temperature T_{ub}, a critical assumption in the Thellier-Thellier method.

[41] The "In-field, zero-field" (IZ) experiment [e.g., *Aitken et al.*, 1988] reverses the order in which the rema-nences are measured. The specimen is first heated to some temperature (e.g., T_2) in Figure 11 and cooled in B_{lab}, then reheated to T_2 and cooled in zero field. The pTRM check step can be performed after the zero field step, but the pTRM tail check step is not possible.

[42] We used the "IZZI" experimental approach for our preliminary study of the metallurgical slag described by *Tauxe and Staudigel* [2004] and *Yu et al.* [2004]. (In fact, this procedure was first applied to these slags.) We combine the IZ and the ZI protocols by alternating between them in the experiment shown in Figure 11. The "IZZI" method incorporates the advantages of both protocols, allowing most of the key assumptions in the Thellier method to be more thoroughly tested with no increase in experimental effort.
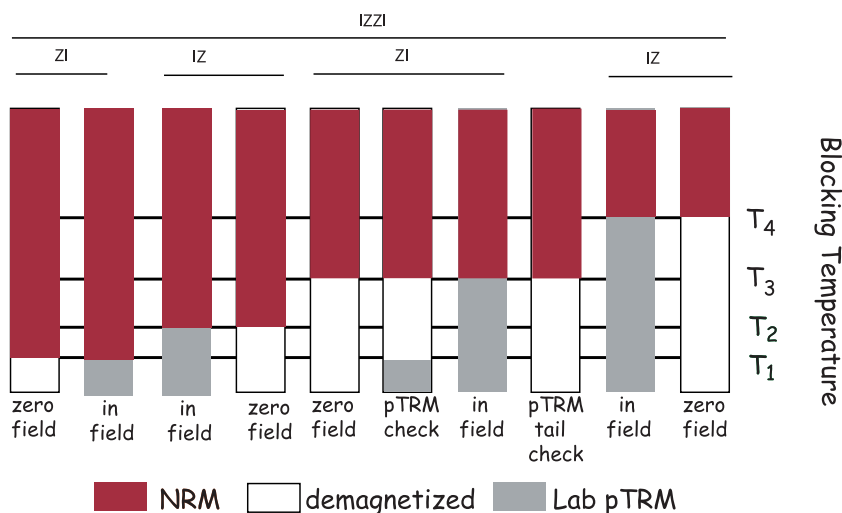
Figure 11. Schematic diagram of the IZZI experimental protocol (see text).

[43] The paleointensity experiment requires that the magnetic grains within the sample be small enough such that the magnetizations within the grains are subparallel (flower remanence state [*Schabes and Bertram*, 1988]) as opposed to "swirling" (vortex remanence state [*Schabes and Bertram*, 1988]) or dividing into magnetic domains separated by domain walls. For magnetite, the width of the magnetic particles should be less than about 100 nm [see, e.g., *Tauxe et al.*, 2002].

[44] Every material studied for paleointensity behaves differently and there is no "magic bullet" set of statistics that guarantees the quality of the data chosen. Nonetheless, there are statistics that describe the behavior and are designed to test the fundamental assumptions of the paleointensity experiments. We find the following statistics useful [see also *Tauxe et al.*, 2006, Table 2].

[45] ● The "scatter" statistic β: the standard error of the slope σ (assuming uncertainty in both the pTRM and NRM data) over the absolute value of the best fit slope $|b|$ [*Coe et al.*, 1978].

[46] ● The Deviation of the ANGle (DANG [*Tauxe and Staudigel*, 2004]): The angle that the NRM component used in the slope calculations makes with respect to the origin (see insert to Figure 12a).

[47] ● The Maximum Angle of Deviation (MAD [*Kirschvink*, 1980]): The scatter about the best fit line through the NRM steps.

[48] ● The fraction of the total remanence (by vector difference sum), f_{vds}: *Coe et al.* [1978] proposed the use of the statistic f which is the fraction of the NRM component used in the slope estimation. We find that f works well with single component magnetizations as in Figure 13a where it reflects the fraction of the total NRM used in the slope calculation. However, it is misleading when there are multiple components of remanence as in Figure 12a. The values of f for such specimens can be quite high, whereas the fraction of the total NRM is much less. We prefer to use a statistic f_{vds} [*Tauxe and Staudigel*, 2004] which is the fraction of the total NRM, estimated by the vector difference sum (VDS) of the entire zero field demagnetization data. The VDS (see Figure 12a) "straightens out" the various components of the NRM by summing up the vector differences at each demagnetization step.

[49] ● The Difference RATio Sum, DRATS: The difference between the original pTRM at a given temperature step (horizontal component of the circles in Figure 12) and the pTRM check (horizontal component of the triangles in see Figure 12), δ_i (see Figure 12a), can result from experimental noise or from alteration during the experiment. *Selkin and Tauxe* [2000] normalized the maximum δ_i value within the region of interest by the length of the hypotenuse of the NRM/pTRM data used in the slope calculation. DRAT is therefore the maximum difference ratio. In many cases, it is useful to consider the trend of the pTRM checks as well as their maximum deviations. We follow *Tauxe and Staudigel* [2004] and use the sum of these differences. We normalize this difference sum by the pTRM acquired by cooling from the maximum temperature step used in the slope calculation to room temperature. This statistic is called the Difference RATio Sum or DRATS.

[50] ● Maximum Difference percentage MD%: The absolute value of the difference between the original NRM measured at a given temperature step (vertical component of the circles in Figure 12) and the second zero field step (known as the pTRM tail check) results from some of the pTRM imparted in the laboratory at T_i having unblocking temperatures that are greater than T_i. These differences (Δ_i, see Figure 12b) are plotted as squares. The Maximum Difference, normalized by the VDS of the NRM and expressed as a percentage is the statistic MD%.

[51] ● Zig-Zag Z: In certain specimens, the IZZI protocol leads to rather interesting behavior, described in detail by *Yu et al.* [2004]. The solid symbols in Figure 12 are the zerofield-infield (ZI) steps and the intervening steps are the infield-zerofield (IZ) steps (open circles). Alternating the two results in a "zigzag" in some specimens. The zigzag can be in either the Arai [*Nagata et al.*, 1963] diagrams (compare slope of solid versus dashed line segments in Figure 12b) or in the orthogonal projections or the zero field vectors (compare directions of solid and dashed line segments in Figure 12c). We therefore can define a statistic Z by testing the difference in either the two sets of slopes or the two sets of directions between the IZ steps and the ZI steps.

[52] To test the significance of the difference between the zero-field IZ directions and those from the ZI zero-field steps, we calculate F test (F_w) for Watson's test for common mean [*Watson*, 1983]. The zigzag for directions Z_{dir} is ratio $F_w/F_{(\nu)}$ where $F_{(\nu)}$ is the critical value for F at $\nu = 2N - 2$ degrees of freedom (at the 95% level of confidence). For the slopes, we calculate the mean and variance of the slopes for the IZ segments ($\bar{b}_{iz}, \sigma_{iz}^2$) and the ZI segments ($\bar{b}_{zi}, \sigma_{iz}^2$). The statistic t_b is the t test for the two means. The zigzag for the slopes Z_{slope} is the ratio $t_b/t_{(\nu)}$ where $t_{(\nu)}$ is critical value for t with $\nu = N_{iz} + N_{zi} - 2$ degrees of freedom (from a statistics table).

[53] If the difference between the sets of directions and slopes is less than 3° or both Z_{slope} and Z_{dir} are less than unity, then Z = 0. Otherwise Z is the larger of Z_{dir} and Z_{slope}.

8.2. Interpretation of Paleointensity Data

[54] Interpretation of paleointensity experimental data in terms of the ancient geomagnetic field relies on the identification of the correct slope in the Arai plots. The experimental results shown in Figure 12 were chosen to illustrate various forms of pathological behavior and have no geomagnetic significance. Many of our slag experiments were much better behaved (see for example Figure 13a). Yet even relatively "well behaved" experiments can be open to interpretation if the data in the Arai plot do not make a single straight line. Curved or multicomponent Arai plots (as in Figures 13c and 13e) can result from (1) multi component NRMs (see inset to Figure 13c) one of which may be an original TRM; (2) failure of the reciprocity of blocking and unblocking; and/or (3) alteration during the experiment. The experimental results shown in Figures 13c–13f are typical of these more ambiguous experimental data. The Arai plots shown in Figure 13c and e both are nonlinear and could be interpreted as two line segments, one of which might relate to the ancient geomagnetic field. In the inset to Figure 13c, there are two directional components, related also to "kinks" in the demagnetization diagram in Figure 13d. Here we feel justified in selecting the second (higher temperature) slope in the Arai plot as the original TRM
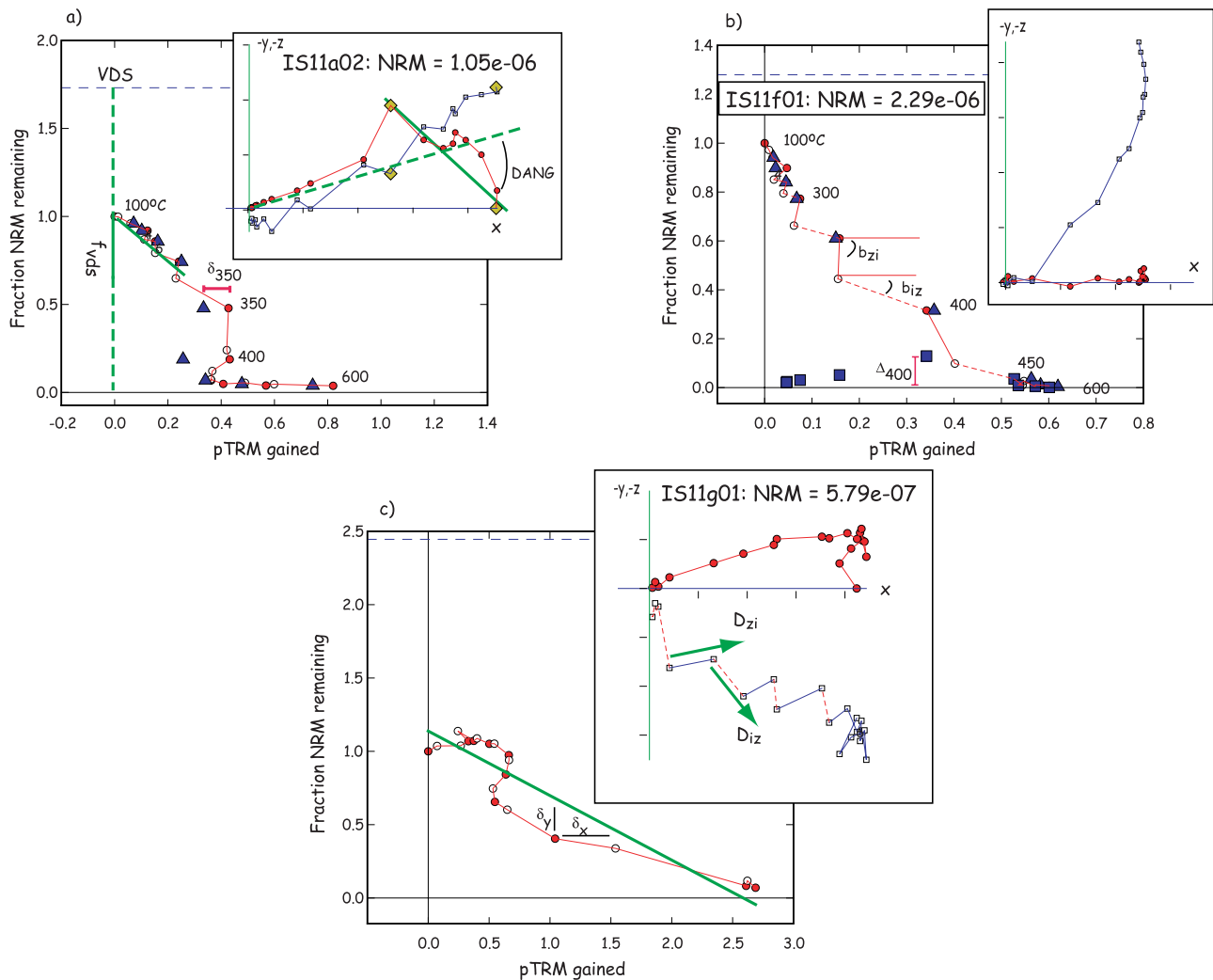
Figure 12. Illustration of paleointensity statistics and pathologies. Arai plots: The magnitude of the NRM remaining after each step is plotted versus the pTRM gained at each temperature step. Closed symbols are zero-field first followed by in-field steps (ZI) while open symbols are in-field first followed by zero field (IZ). Triangles are pTRM checks and squares are pTRM tail checks. Horizontal dashed lines are the vector difference sum (VDS) of the NRM steps. Vector endpoint plots: Insets are the x, y (solid symbols) and x, z (open symbols) projections of the (specimen coordinates) natural remanence (zero field steps) as it evolves from the initial state (plus signs) to the demagnetized state. The laboratory field was applied along -Z. Diamonds indicate bounding steps for calculations. (a) The f_{vds} is the fraction of the component used of the total VDS. The difference between the pTRM check and the original measurement at each step is δT_i. The inset shows the deviation angle (DANG) that a component of NRM makes with a line going through the origin. The maximum angle of deviation MAD is calculated from the scatter of the points about the best fit line (solid green line). (b) Data exhibit zig-zag behavior diagnostic for significant difference between blocking and unblocking temperatures. The Zig-zag for slopes compares slopes calculated between ZI and IZ steps (b_{zi}) with those connecting IZ and ZI steps b_{zi}). The difference between the pTRM tail check and the original measurement at each step is ΔT_i. (c) β reflects the scatter (δ_x, δ_y) about the best fit slope (solid green line). The Zig-zag for directions compares those calculated between ZI and IZ steps (D_{zi}) with those connecting IZ and ZI steps (D_{zi}). See text.

component. However, in Figure 13e there is only one directional and blocking temperature component and we do not have a straightforward way of choosing which slope in the Arai plot is the "correct" one; in cases like this we choose the entire range for the slope selection, resulting in a very large scatter statistic and ultimate rejection of this specimen.

[55] We have interpreted all experimental data in a consistent manner, relying heavily on the vector end-point and demagnetization diagrams to guide our selection of slopes. Our entire data set as well as our interpretations are available in the MagIC database (persistent link http://earthref.org/
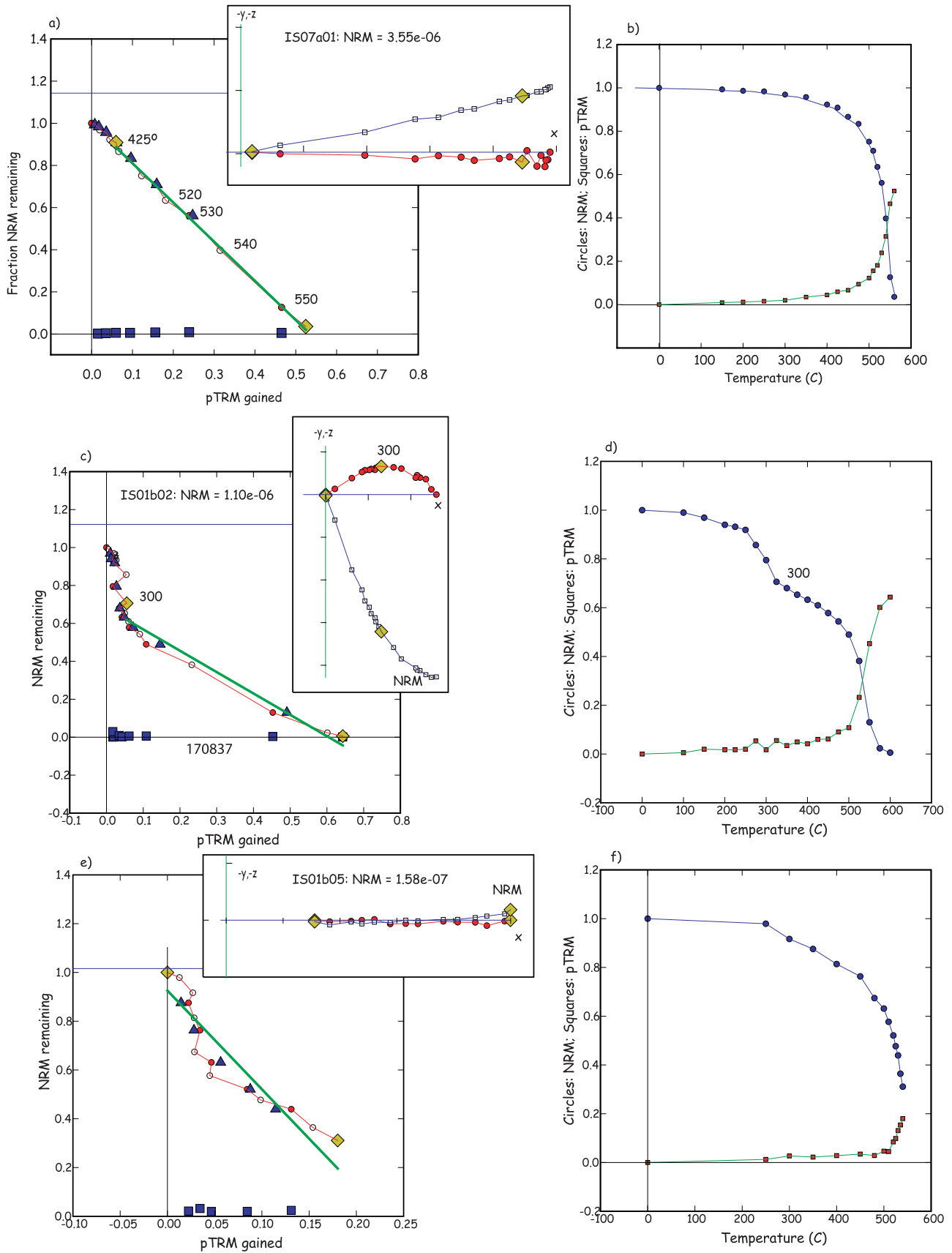
Figure 13

Table 3. Summary of Acceptance Criteria[a]

$\sigma\%$	DRATS	MD%	Z	β	f_{vds}	MAD	DANG	N_{samps}
10.0	18.0	5.0	2.0	0.08	0.5	5.0	7.0	16
20.0	20.0	7.0	2.0	0.15	0.3	7.0	9.0	27

[a]$\sigma\%$: standard deviation cut-off expressed as percentage of mean of specimens per sample. N_{samps}: number of samples meeting these criteria.

cgi-bin/magic.cgi?mdt = m000629dt20080303183541) for inspection.

9. AARM

[56] A few specimens are highly anisotropic. We used the method described by *Selkin et al.* [2000] which relies on the anisotropy of anhysteretic remanence (AARM) tensor to correct our paleointensity results for the effects of TRM anisotropy. An ARM was imparted in nine directions after demagnetization in an alternating field of 180 mT prior to each ARM. The nine values of ARM were reduced to a best fit tensor using Hext statistics [*Hext*, 1963] and this AARM tensor was used to correct the intensity values for the specimen. Unfortunately many specimens were destroyed to make hysteresis measurements before the need for an anisotropy correction was realized, so anisotropy of anhysteretic remanence measurements were made on only 81 specimens. Anisotropy corrected values are flagged with the method code DA-AC-AARM (data adjustment-anisotropy correction-AARM) in the specimen record uploaded to the MagIC database.

[57] Ideally, one would do the AARM test on every specimen, but that is now impossible. Comparing corrected versus uncorrected intensity estimates, the average difference between the two is 4.4% ±6.1. The difference ranges from 0 to 45% however, so while the average correction is small the potential error is large. Moreover, we hesitate to mix corrected and uncorrected estimates in the same average. To deal with this issue, we averaged specimen data by sample using first only the anisotropy uncorrected data, and then only anisotropy corrected data. For each sample, the set of data yielding the lowest standard deviation was used (either all corrected, or all uncorrected). Because the correction varies from specimen to specimen and can be either positive or negative, uncorrected data that require anisotropy corrections that are not available will have high internal scatter because specimens were randomly oriented with respect to each other and the lab field direction. This is the underlying rationale for basing our selection criteria on internal reproducibility, which should exclude biased results.

9.1. Cooling Rate Effect

[58] It is well known that differences in laboratory and original cooling rates affect the estimate of paleofield intensity [e.g., *Halgedahl et al.*, 1980]. If, for example, the material of interest cooled over a day during initial fabrication and cooled over an hour in the laboratory, the ancient geomagnetic field could be over-estimated by as much as 10–20%, depending on blocking temperature (lower blocking temperatures result in higher over-estimates). For some pottery fragments, the overestimation was shown experimentally to be as much as 15–20% with an original cooling time of a day (from the Curie temperature) and an experimental cooling time of half hour [*Genevey and Gallet*, 2002]. Therefore it is important to have some idea about the relative cooling rates during initial slag formation and laboratory cooling rates during the in-field cooling steps. For the latter, the samples cooled over a period of 0.5–1 h (depending on temperature step). For the former, we draw on reconstructions of the copper smelting process [e.g., *Merkel*, 1990; *Hauptmann*, 2000]. As already mentioned, tapping slag is poured out on the ground and is rapidly quenched, with cooling rates likely to be comparable to laboratory conditions. However, furnace slag cools inside the furnace and is likely to have cooled slower than the tapping slag. Nonetheless, the furnaces were frequently broken apart so that the smelters could have rapid access to the slag and the copper prills embedded in it. Even if the furnaces were left intact and the slag allowed to cool in situ, the furnaces are quite small (generally at most a half meter in diameter) and the slag material would have been cool to the touch within a few hours. The "worst case" overestimate of ancient field would be for the copper-magnesian ferrites with low blocking temperatures (∼300°C) and several times slower cooling rate than in the laboratory. That could result in an overestimate of a few percent at most. Therefore we have not corrected our ancient intensity estimates for the effect of cooling rate.

9.2. Cut-off Values

[59] The decision on threshold values for the variety of paleointensity statistics has been extremely subjective. In this paper, we have tried to minimize the subjective nature of setting cutoff values by simply finding the set of cutoff values that yield the maximum number of samples with at least three specimens with standard deviations that met either a given standard deviation expressed as the percent of the mean. Here we consider results using two standard deviation cutoffs: 10%, and 20%. [Because of bias introduced at low intensities by setting a strict percentage based cutoff, we do not exclude results with standard deviations less than 5 μT.] The set of statistics that yielded the most consistent results at a sample level for a given standard deviation cutoff is shown in Table 3.

[60] Specimens were assigned "grades" as follows: If all criteria were met, the specimen was given a grade of "A". Those that failed one criterion were given a "B", two a "C" and so on. The criterion that was not met in grade "B"

Figure 13. Illustration of interpretation of paleointensity data. Figures 13a, 13c, and 13e are Arai plots as in Figure 12. Insets are vector end-point plots as in Figure 12. Figures 13b, 13d, and 13f are NRM intensity decay curves, as a function of zero field demagnetization step. Figure 13a and Figure 13b are from a specimen whose interpretation is straight-forward. Figure 13c and Figure 13d are data from a specimen displaying two NRM components, evident in the directional change in the inset to Figure 13c and the "roller coaster" behavior in the intensity decay curve in Figure 13d. Figure 13e and Figure 13f shows an experiment with a two component Arai plot (Figure 13e) with a single component vector end-point diagram (inset).
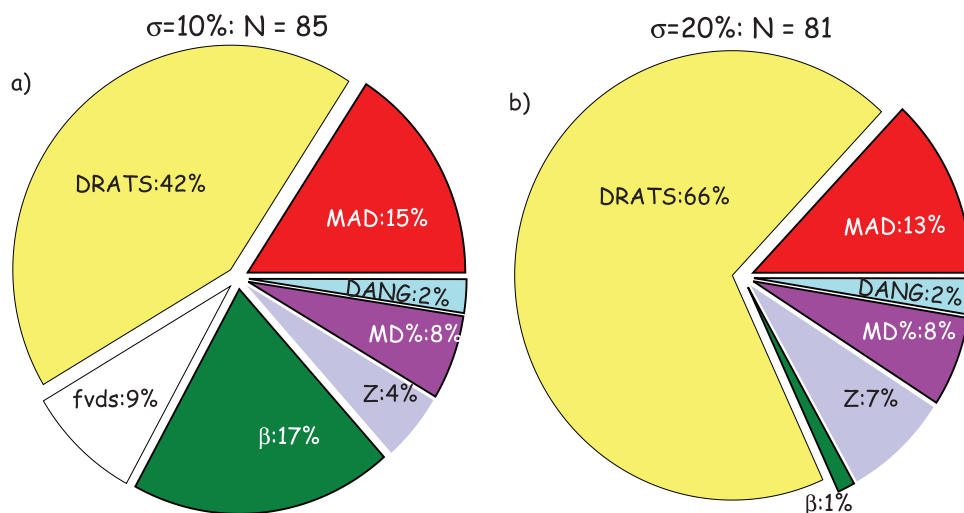
Figure 14. Pie charts with cause of failure for grade "B" specimens for the two standard deviation cutoffs used in this paper.

specimens is shown in Figure 14 for each standard deviation cutoff. The most efficient statistic for improving consistency at a sample level is always the alteration check statistic (DRATS). Therefore most specimens that were eliminated, were rejected because they exhibited alteration during the experiment.

[61] In the following we will consider two sets of criteria: the "strict" set using those optimizing the results using a standard deviation cutoff of 10%, and a "loose" set, optimizing results with a standard deviation cutoff of 20%. A minimum of three specimens per sample was required for both sets of criteria.

10. Results

10.1. Remelted Slag Samples

[62] Representative results from our synthetic slag specimens are shown in Figure 15. Most of the specimens made of partially molten furnace slag (IS12a, Figures 15a and 15b) behaved very poorly during the paleointensity experiment, with acquisition of a magnetization parallel to the laboratory field indicating extensive alteration during the "paleointensity" experiment. The behavior was unlike any of the results observed from archaeological slag. The fully remelted tapping slag sample (IS13a, Figures 15c and 15d), however, behaved much more like the archaeological samples studied here. There is a single component of magnetization with a blocking temperature spectrum similar to the original slag from which it was taken. Treating the data for the synthetic specimens in the same manner as for the archaeological slag (using the loose criteria) results in an average intensity of 36.6 ± 3 μT for sample IS13a, in excellent agreement with the measured field, 35.9 ± 0.1 μT in the laboratory. IS12a did not have any specimens meeting our acceptance criteria.

10.2. Archaeointensity Results

[63] A total of 207 out of 400 specimens gave a "grade A" results using the "loose" selection criteria while 154 met the "strict" criteria. The sample means from specimens meeting the strict and loose criteria are listed in Tables 4

and 5 respectively. [Note that only those not listed in Table 4 appear in Table 5.] Of these 17 had standard deviations of the mean less than 5 μT or 10% of the mean while 33 had standard deviations of the mean less than 5 μT or 20% of the mean. Our success rate on a per sample basis was therefore 21.5% and 41.8% based on the strict and loose criteria respectively.

[64] Our results are summarized in Figure 16. In Figure 16a, we show the sample means based on the two sets of criteria, strict (circles) and loose (diamonds) for samples from a well dated archaeological context (age quality of 2 or better in Table 2). For context, we plot the recently published data set from archaeointensity investigation of Northern Levantine Syrian sites [*Genevey et al.*, 2003; *Gallet and Le Goff*, 2006; *Gallet et al.*, 2006], obtained under rigorous experimental conditions and careful archaeological context together with the predicted VADM for the region from the CALS7K.2 model of *Korte and Constable* [2005a]. Data meeting the 20% standard deviation cut-off (or 5 μT) whose ages are poorly constrained are shown as triangles in Figure 16b.

11. Discussion

11.1. Data Reliability

[65] The sources of nonideal behavior in these (and most) paleointensity experiments are (1) alteration during laboratory heating, (2) multicomponent behavior of the NRM, (3) pTRM tails resulting from inequality of blocking and unblocking temperature, (4) inadequate correction for the anisotropy of TRM acquisition. Considering that we made no attempt to preselect samples using rock magnetic data (e.g., reversible thermomagnetic experiments or hysteresis behavior), we rely on reproducibility at the cooling unit (sample) level as the primary basis for acceptance or rejection of a given paleointensity estimate. This approach had a $21-42\%$ success rate (depending on the tolerance set for the criteria).

[66] The key question in this study is whether the results that pass our two stage selection process (specimen and sample level) are in fact reliable. Three observations support the claim that they are reliable: (1) comparison of different
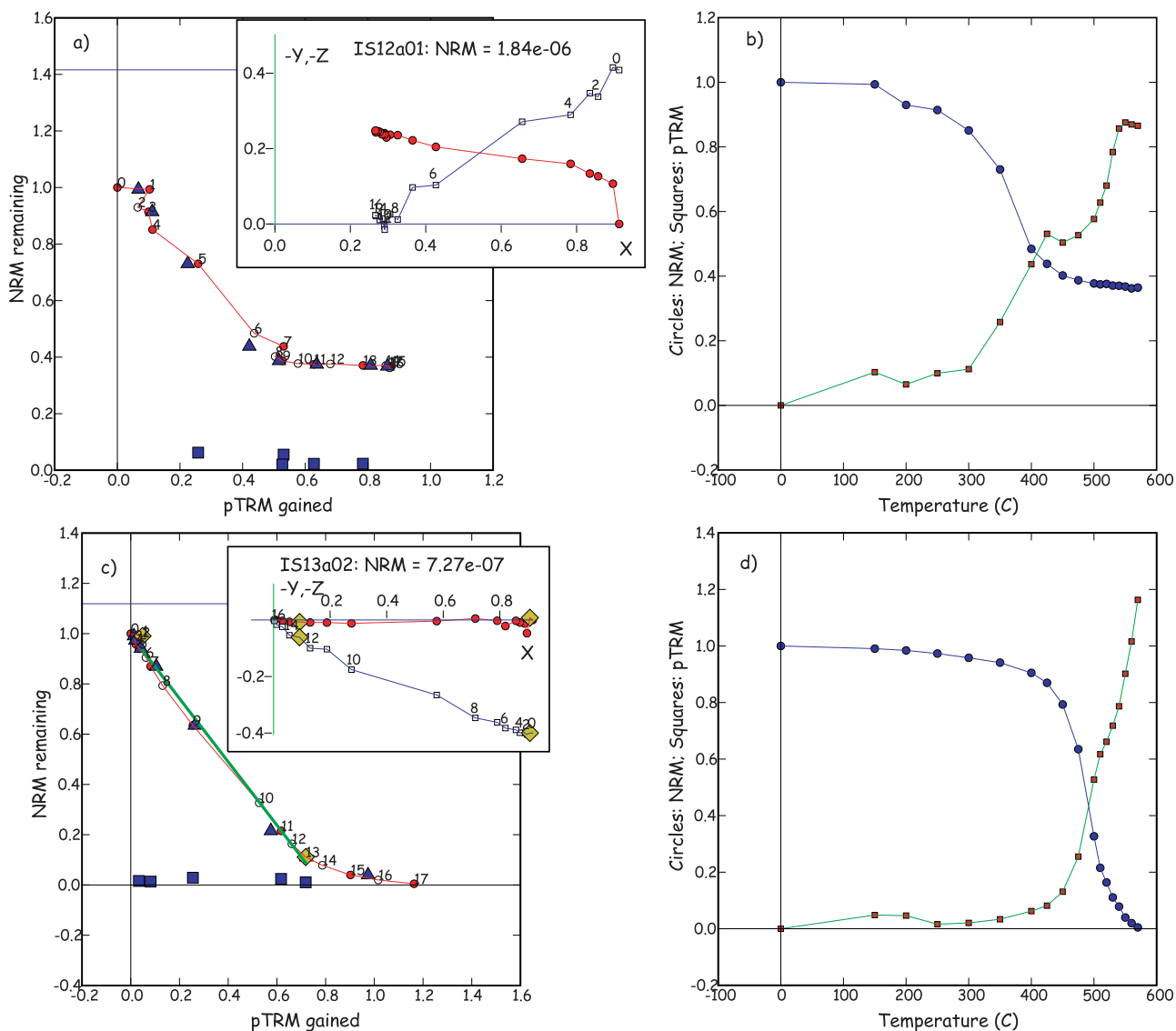
Figure 15. Representative results from IZZI experiments on two remelted specimens (symbols as in Figure 12).

recording media of clay and furnace slag, (2) comparison of results from the same well constrained age, (3) agreement of our results with those from Syria, and (4) the results of the remelting experiment done in known field.

[67] The detailed results of clay/furnace slag pairs are listed in Table 6. We tested four clay samples of which all passed our selection criteria. IS14b (furnace slag) unfortunately had only one specimen that was usable (IS14b04), but it had a paleointensity estimate of 33 μT, in excellent agreement with the average of the clay sample (IS14c) of 31 $\pm$ 2 μT. IS20c was a single piece that comprised both furnace clay (IS20c01-07) and slag (IS20c08-11). The results from these specimens calculated separately are statistically indistinguishable. Two other examples (JS01b/c and JS04a/b) also show consistency between clay and furnace slag although JS01c is statistically distinct from JS01b. Therefore furnace slag yields results compatible with furnace clay in all cases tested.

[68] IS05a, IS06a and IS06b all come from the same well constrained age interval, passed our selection criteria and agree with one another within the uncertainty (see Figure 16a and Tables 4 and 5). Two other examples of samples from the same age are shown in Figure 16b, but the absolute age is poorly known (IS02a, e, f and IS01a, b, IS20c). These samples are in excellent agreement with one another, although not with their expected intensities, an observation we ascribe to poor age constraints. The single example of samples from the same site with very poor internal agreement is IS11, whose age is quite controversial. We argue that this site actually contains samples ranging in age from about 6000 years ago to as young as 3000 years ago.

[69] As shown in Figure 16a, the samples which pass our two stage selection process whose ages are well constrained show excellent agreement with results from Syria of *Genevey et al.* [2003], *Gallet and Le Goff* [2006], and

Table 4. Summary of Sample Averages of Grade A Specimens, Using the "Strict" (10% σ) Criteria in Table 3 as Explained in Text[a]

Sample	Latitude/Longitude	Age	σ	Q	N	B (μT)	σ	σ%	VADM (ZAm^2)	σ
IS01a	29.8300/35.0200	5350	1100	5	1	56.9	0.0		111.2	0.0
IS01b	29.8300/35.0200	5350	1100	5	1	56.3	0.0		110.1	0.0
IS02a	29.7922/35.0015	4100	150	6	3	58.3	1.1	1.9	114.0	2.2
IS02e	29.7922/35.0015	4100	150	6	3	55.3	7.4	13.4	108.2	14.4
IS02f	29.7922/35.0015	4100	150	6	4	54.6	4.6	8.4	106.8	9.0
IS03a	29.7922/35.0015	4100	150	2	1	84.1	0.0		164.5	0.0
IS03b	29.7922/35.0015	4100	150	2	4	43.0	3.6	8.3	84.1	7.0
IS04b	29.7164/34.9841	1100	150	2	4	54.7	3.1	5.6	107.2	6.0
IS05a	29.7840/34.9477	3175	75	2	3	61.9	1.7	2.7	121.2	3.3
IS06a	29.7840/34.9477	3175	75	2	6	61.1	6.8	11.2	119.6	13.4
IS06b	29.7840/34.9477	3175	75	2	3	56.8	5.1	9.0	111.1	10.0
IS07a	29.7173/34.9851	3735	20	2	3	56.1	1.2	2.2	109.9	2.4
IS07b	29.7173/34.9851	3735	20	2	7	42.9	10.6	24.8	84.0	20.8
IS07d	29.7173/34.9851	3735	20	2	1	54.0	0.0		105.7	0.0
IS08a	29.7786/34.9519	3175	75	2	2	64.2	1.6	2.6	125.7	3.2
IS08b	29.7786/34.9519	3175	75	2	4	74.4	37.1	49.8	145.6	72.5
IS08c	29.7786/34.9519	3175	75	2	3	52.7	8.3	15.7	103.2	16.1
IS09a	29.7713/34.9467	2810	60	3	1	55.2	0.0		108.0	0.0
IS10a	29.5891/34.9647	1150	150	3	1	16.4	0.0		32.2	0.0
IS10b	29.5891/34.9647	1150	150	3	1	37.6	0.0		73.7	0.0
IS10c	29.5891/34.9647	1150	150	3	1	15.4	0.0		30.3	0.0
IS10e	29.5891/34.9647	1150	150	3	3	65.4	11.0	16.8	128.3	21.6
IS11b	29.7624/34.9943	6150	250	6	2	57.1	0.6	1.0	111.7	1.1
IS11c	29.7624/34.9943	6150	250	6	4	47.9	16.5	34.4	93.7	32.2
IS11d	29.7624/34.9943	6150	250	6	3	76.3	4.1	5.4	149.3	8.0
IS11e	29.7624/34.9943	6150	250	6	1	30.3	0.0		59.3	0.0
IS11h	29.7624/34.9943	6150	250	6	1	52.2	0.0		102.1	0.0
IS11i	29.7624/34.9943	6150	250	6	5	49.7	4.7	9.5	97.3	9.3
IS14c	31.1947/34.6601	6225	50	1	3	30.5	1.9	6.1	58.7	3.6
IS15a	29.8852/35.0458	4600	350	5	3	67.7	1.7	2.5	132.2	3.4
IS16a	29.8852/35.0458	1950	100	1	4	36.9	9.0	24.4	72.2	17.6
IS17a	29.8897/35.0582	5810	500	3	8	36.7	7.0	18.9	71.7	13.6
IS18a	29.6477/34.9388	1150	150	6	6	44.3	4.5	10.1	86.8	8.8
IS19a	29.5891/34.9524	4600	350	5	2	36.5	1.5	4.1	71.7	2.9
IS20c	31.6795/34.5556	5425	125	4	9	55.8	9.0	16.1	106.6	17.1
IS21a	32.0915/34.8064	3050	100	3	3	45.7	1.8	4.0	86.8	3.5
IS22a	32.6168/34.9160	3050	100	1	2	68.1	19.9	29.2	128.5	37.5
IS24a	29.7624/34.9943	6150	250	6	1	78.5	0.0		153.6	0.0
IS25a	29.6947/34.9872	1150	150	3	3	24.0	12.6	52.3	47.1	24.6
JS01c	30.6727/35.3846	5200	250	1	5	28.7	1.6	5.4	55.5	3.0
JS02a	30.7071/35.4522	2980	110	1	3	52.4	24.2	46.2	101.4	46.8
JS02b	30.7071/35.4522	2980	110	1	3	82.8	6.0	7.2	160.1	11.6
JS04a	30.6286/35.4972	4550	300	1	3	51.6	11.2	21.8	99.9	21.7
JS04b	30.6286/35.4972	4550	300	1	3	51.3	0.7	1.4	99.3	1.4
JS05a	30.6753/35.4467	700	50	1	3	43.4	1.8	4.1	83.9	3.4
JS08a	30.6630/35.3932	4050	100	1	5	35.5	5.3	14.8	68.6	10.2

[a]Ages are in Cal BP. Q refers to the age quality as in Table 2.

Gallet et al. [2006]. We take this as strong encouragement that our selection process rejects unreliable data.

[70] Finally, we made slag under known conditions of the geomagnetic field. The single sample that passed all our selection criteria yielded an intensity estimate consistent with the field, providing further support for the reliability of our selection process. We conclude therefore that copper slag material can be well suited for archaeointensity determination.

11.2. Comparison of Different Sample Types

[71] Comparing the experimental behavior of specimens from the two main groups of copper slag shows little difference in terms of success rate, with a very slight preference toward furnace slag (Figure 17). This is somewhat surprising because we expected the tapping slag specimens, which are more homogenous and glassy, to show better experimental behavior. The difference might be caused by alteration associated with the abundant charcoal embedded in many of the tapping slag samples. This alteration of the original slag material is visible in many tapping slag samples, and the most charcoal-rich samples failed our selection criteria completely (e.g., JS03). The dating possibilities of charcoal-rich slag samples is a key factor in the future potential of slag archaeointensity research, therefore we plan to investigate further the connection between the charcoal and mineralogical alteration. Tapping slag samples are usually large enough to contain sufficient unaltered material within the same sample with some effort.

[72] Another observation regarding the experimental behavior of copper slag specimens might suggest a difference between samples that originated in the Timna region versus samples that originated in Faynan region. The former show greater success rate (by a factor of 2), although, given the relatively small number of specimens from Faynan, this

**Table 5.** Summary of Sample Averages of Grade A Specimens Using the "Loose" (20% σ) Criteria in Table 3[a]

Sample	Latitude/Longitude	Age	σ	Q	N	B (μT)	σ	σ%	VADM (ZAm^2)	σ
IS01a	29.8300/35.0200	5350	1100	5	3	57.8	7.8	13.5	113.1	15.3
IS01b	29.8300/35.0200	5350	1100	5	4	59.7	5.5	9.2	116.8	10.8
IS01e	29.8300/35.0200	5350	1100	5	2	22.3	10.4	46.7	43.6	20.4
IS01f	29.8300/35.0200	5350	1100	5	1	54.4	0.0		106.3	0.0
IS02a	29.7922/35.0015	4100	150	5	3	58.3	1.1	1.9	114.0	2.2
IS02e	29.7922/35.0015	4100	150	5	5	55.0	7.1	12.9	107.6	13.9
IS02f	29.7922/35.0015	4100	150	5	7	54.0	4.6	8.5	105.7	9.0
IS03a	29.7922/35.0015	4100	150	2	4	81.5	31.5	38.6	159.5	61.5
IS03b	29.7922/35.0015	4100	150	2	3	43.7	4.4	10.1	85.4	8.6
IS04b	29.7164/34.9841	1100	150	2	5	52.2	6.2	12.0	102.2	12.2
IS05a	29.7840/34.9477	3175	75	2	3	61.9	1.7	2.7	121.2	3.3
IS06a	29.7840/34.9477	3175	75	2	6	61.1	6.8	11.2	119.6	13.4
IS06b	29.7840/34.9477	3175	75	2	4	55.3	5.2	9.3	108.1	10.1
IS07a	29.7173/34.9851	3735	20	2	3	56.1	1.2	2.2	109.9	2.4
IS07b	29.7173/34.9851	3735	20	2	9	42.6	9.7	22.8	83.4	19.0
IS07d	29.7173/34.9851	3735	20	2	1	54.0	0.0		105.7	0.0
IS08a	29.7786/34.9519	3175	75	2	2	64.2	1.6	2.6	125.7	3.2
IS08b	29.7786/34.9519	3175	75	2	6	64.2	33.3	51.9	125.6	65.2
IS08c	29.7786/34.9519	3175	75	2	4	49.6	9.2	18.6	97.0	18.0
IS09a	29.7713/34.9467	2810	60	3	3	64.0	11.6	18.1	125.3	22.7
IS10a	29.5891/34.9647	1150	150	3	2	27.8	16.1	57.8	54.5	31.5
IS10b	29.5891/34.9647	1150	150	3	1	37.6	0.0		73.7	0.0
IS10c	29.5891/34.9647	1150	150	3	3	26.1	21.5	82.3	51.2	42.1
IS10d	29.5891/34.9647	1150	150	3	1	22.1	0.0		43.3	0.0
IS10e	29.5891/34.9647	1150	150	3	4	63.1	10.1	16.1	123.7	19.9
IS11b	29.7624/34.9943	6150	250	6	3	54.6	4.3	8.0	106.8	8.5
IS11c	29.7624/34.9943	6150	250	6	5	52.4	17.4	33.3	102.5	34.1
IS11d	29.7624/34.9943	6150	250	6	4	73.9	5.8	7.9	144.6	11.4
IS11e	29.7624/34.9943	6150	250	6	4	34.0	3.4	10.0	66.5	6.7
IS11f	29.7624/34.9943	6150	250	6	1	84.5	0.0		165.4	0.0
IS11h	29.7624/34.9943	6150	250	6	1	52.2	0.0		102.1	0.0
IS11i	29.7624/34.9943	6150	250	6	5	49.7	4.7	9.5	97.3	9.3
IS14b	31.1947/34.6601	6225	50	1	1	33.1	0.0		63.5	0.0
IS14c	31.1947/34.6601	6225	50	1	3	30.5	1.9	6.1	58.7	3.6
IS15a	29.8852/35.0458	4600	350	5	3	67.7	1.7	2.5	132.2	3.4
IS16a	29.8852/35.0458	1950	100	1	3	39.6	6.1	15.5	77.4	12.0
IS17a	29.8897/35.0582	5810	500	3	9	35.9	6.9	19.3	70.1	13.5
IS18a	29.6477/34.9388	1150	150	6	6	44.3	4.5	10.1	86.8	8.8
IS19a	29.5891/34.9524	4600	350	5	3	35.0	2.9	8.3	68.6	5.7
IS20c	31.6795/34.5556	5425	125	4	9	55.8	9.0	16.1	106.6	17.1
IS21a	32.0915/34.8064	3050	100	3	3	45.7	1.8	4.0	86.8	3.5
IS22a	32.6168/34.9160	3050	100	1	3	59.1	21.0	35.5	111.5	39.6
IS24a	29.7624/34.9943	6150	250	6	2	88.5	14.1	16.0	173.1	27.7
IS25a	29.6947/34.9872	1150	150	3	3	24.0	12.6	52.3	47.1	24.6
JS01b	30.6727/35.3846	5200	250	1	4	22.6	1.4	6.4	43.6	2.8
JS01c	30.6727/35.3846	5200	250	1	5	28.7	1.6	5.4	55.5	3.0
JS02a	30.7071/35.4522	2980	110	1	4	47.2	22.4	47.5	91.2	43.3
JS02b	30.7071/35.4522	2980	110	1	3	82.8	6.0	7.2	160.1	11.6
JS04a	30.6286/35.4972	4550	300	1	4	51.9	7.8	15.0	100.3	15.1
JS04b	30.6286/35.4972	4550	300	1	3	51.3	0.7	1.4	99.3	1.4
JS05a	30.6753/35.4467	700	50	1	3	43.4	1.8	4.1	83.9	3.4
JS08a	30.6630/35.3932	4050	100	1	5	35.5	5.3	14.8	68.6	10.2

[a]Ages are in Cal BP. Q refers to the age quality as in Table 2.

observation may not be robust. One of the reasons for any difference between the two regions might derive from the difference in chemical and mineralogical composition of the slag. For example, samples from the Faynan region have manganese as the most abundant metallic component (Table 1). High manganese specimens have lower blocking temperatures in general (see Figure 8) and tend to be more prone to alteration during the experiment.

[73] As discussed in the previous section, we also investigated a few clay samples. All of these samples came from pyrotechnological installations of the copper production industry, thus they were exposed to extremely high temper-

atures (usually above 1200°C). This is different from the more common practice in archaeointensity research, where the clay samples originate from ceramic or mud-bricks fragments, which were exposed to much lower range of temperatures (500–900°C). The experimental results show clearly that clay from pyrotechnological environments are highly suitable for archaeointensity reconstruction. The clay specimens behave well, and the success rate is high (Figure 17). Although the number of clay specimens is much smaller than the number of slag specimens, it is important to note that all of the clay samples had at least two grade "A" specimens with concordant results. We can
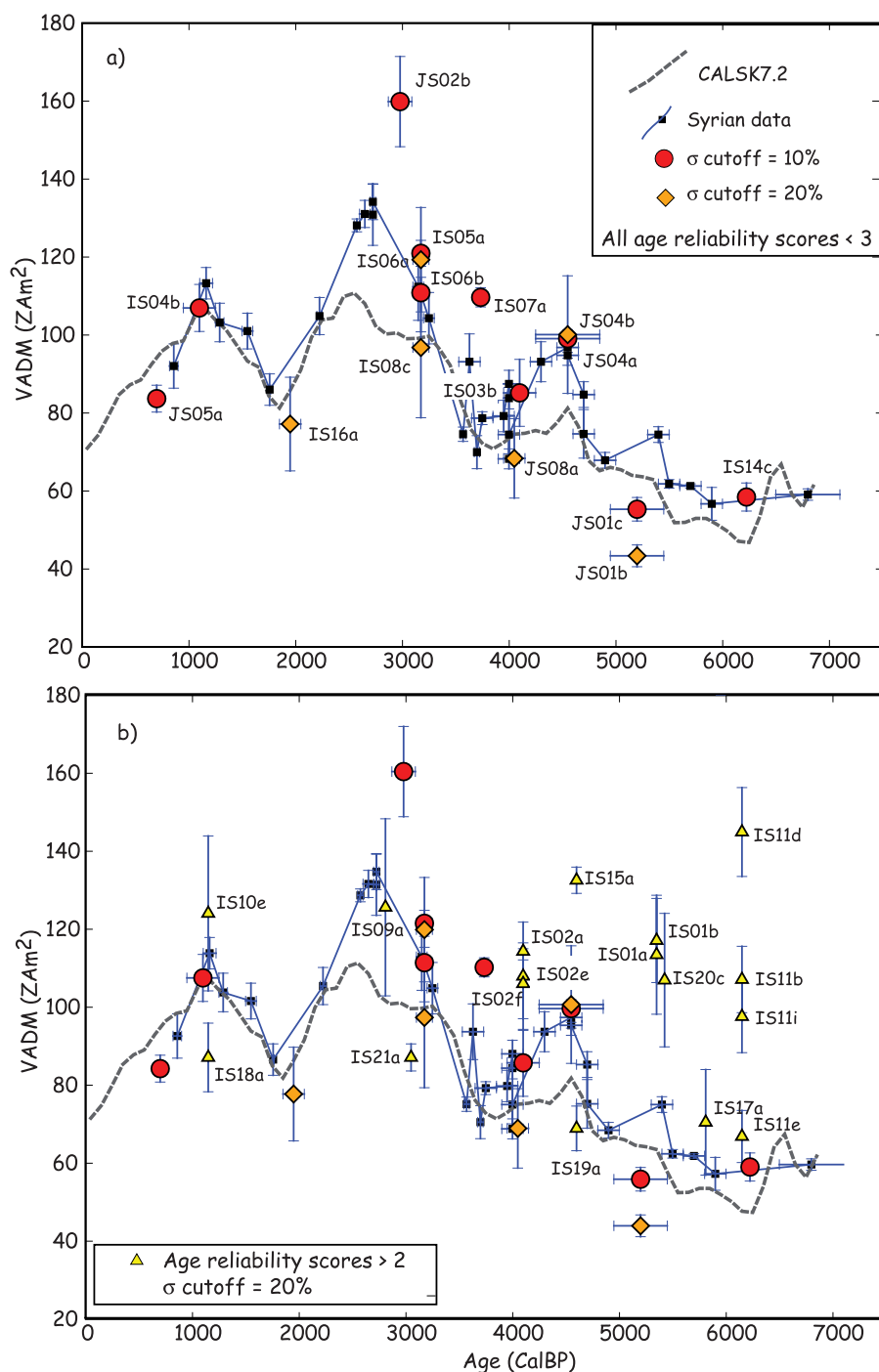
Figure 16. Summary of all acceptable sample intensities (with standard deviation cutoff values of 10% and 20% (Tables 4 and 5) of the mean; $N \geq 3$). (a) All samples have an age reliability index better than 3. (b) Same as in Figure 16a but including samples with uncertain ages. Circles and diamonds have age uncertainties of better than 3, triangles are all others. Small blue squares are data from Syria [*Genevey et al.*, 2003; *Gallet and Le Goff*, 2006; *Gallet et al.*, 2006]. Predicted VADM values for Syria by CALS7K.2 of *Korte and Constable* [2005a] are shown as dashed line.

therefore conclude that this type of material has a great potential for further archaeointensity research.

[74] A few of our specimens originated from bronze slag samples. These are the result of a unique Iron Age I bronze industry that was discovered in numerous sites in the Southern Levant. In the bronze making technique, bronze objects were remelted in ceramic crucibles, in a process that creates slag residues [*Ilan*, 1999]. The experimental results show that bronze slag is suitable as well for archaeointensity experiments (Figure 17), although the number of specimens is too small to allow further conclusions.

Table 6. Comparison of Clay and Furnace Slag Results From Same Sites

Sample/Specimen	Type	N	B, μT	σ
IS14c	clay	3	31	2
IS14b04	FS	1	33	
IS20c01-07	clay	6	59	9
IS20c08-10	FS	3	49	4
JS01b	clay	4	23	1
JS01c	FS	5	29	2
JS04a	FS	4	52	8
JS04b	clay	3	51	1

[75] There is an interesting difference in anisotropy correction between furnace and tapping slag. In general, tapping slag specimens were found to be more anisotropic. The difference between corrected and uncorrected results of tapping slag was 5.3% as in furnace slag it was only 3.7%. This is not surprising, considering the different manufacturing processes and the different corresponding material textures. The connection between embedded textures and anisotropy in archaeointensity samples was already observed in ceramics [e.g., *Aitken et al.*, 1981], where the shaping of the clay enforced mineralogical structures that contribute to the anisotropy of the samples. In our case the evident flow textures observed in tapping slag (Figures 4c and 4d and Figure 10) are likely to be responsible of the higher anisotropy of these samples. Tapping slag, in most cases, cooled as it flowed out onto the ground.

11.3. Levantine Archaeointensity

[76] In Figure 18 we plot a curve derived by combining the Levantine results together (those from Syria in the Northern Levant and our new results from the Southern Levant). Our archaeointensity data from well dated contexts show good agreement with the data set from the Northern Levant [*Genevey et al.*, 2003; *Gallet and Le Goff*, 2006; *Gallet et al.*, 2006]. Comparison between the major trends in the Syria curve and other data sets (e.g., eastern Europe, *Kovacheva et al.* [1998]; Central Asia, *Nachasova and Burakov* [2000]) is available in the work of *Genevey et al.* [2003].

[77] The behavior of the geomagnetic field intensity fluctuated rapidly over the last 7000 years. There is a
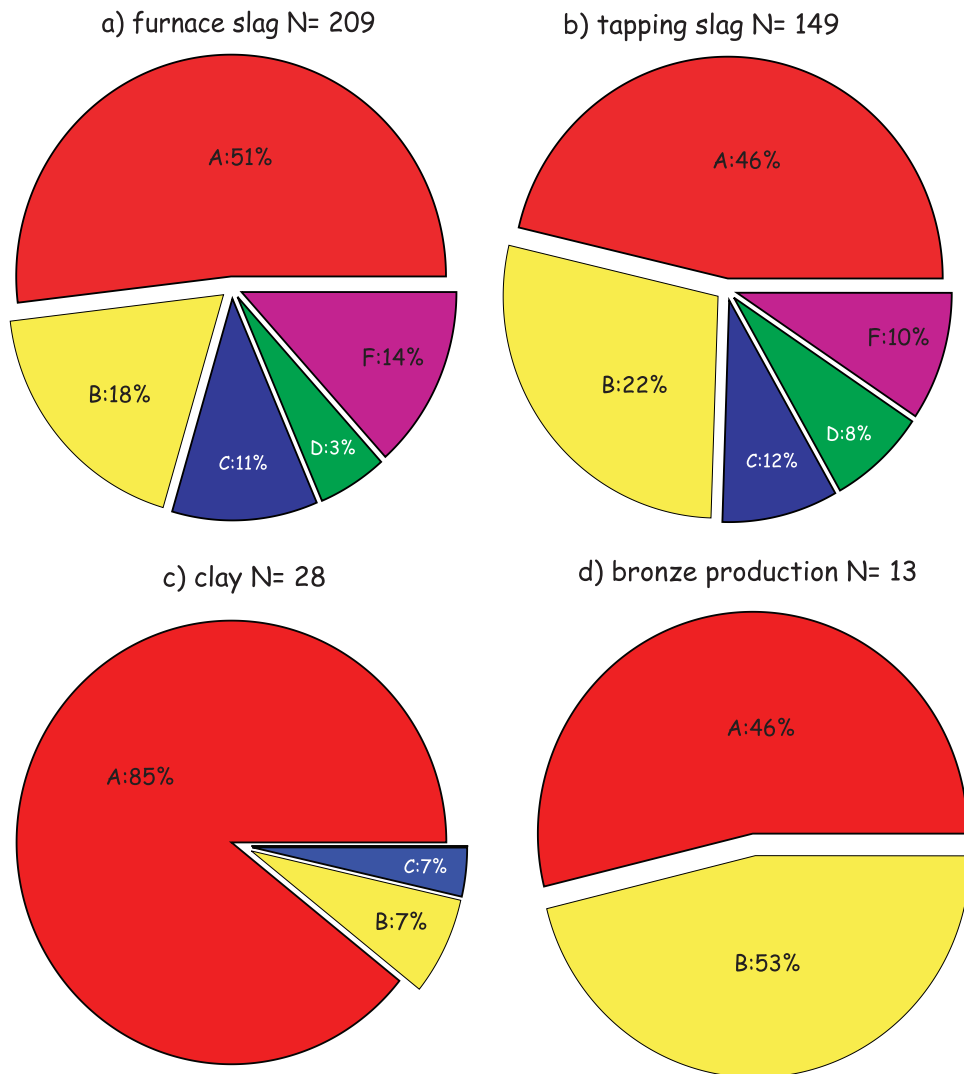
Figure 17. Success rate for various specimen types (Loose criteria).
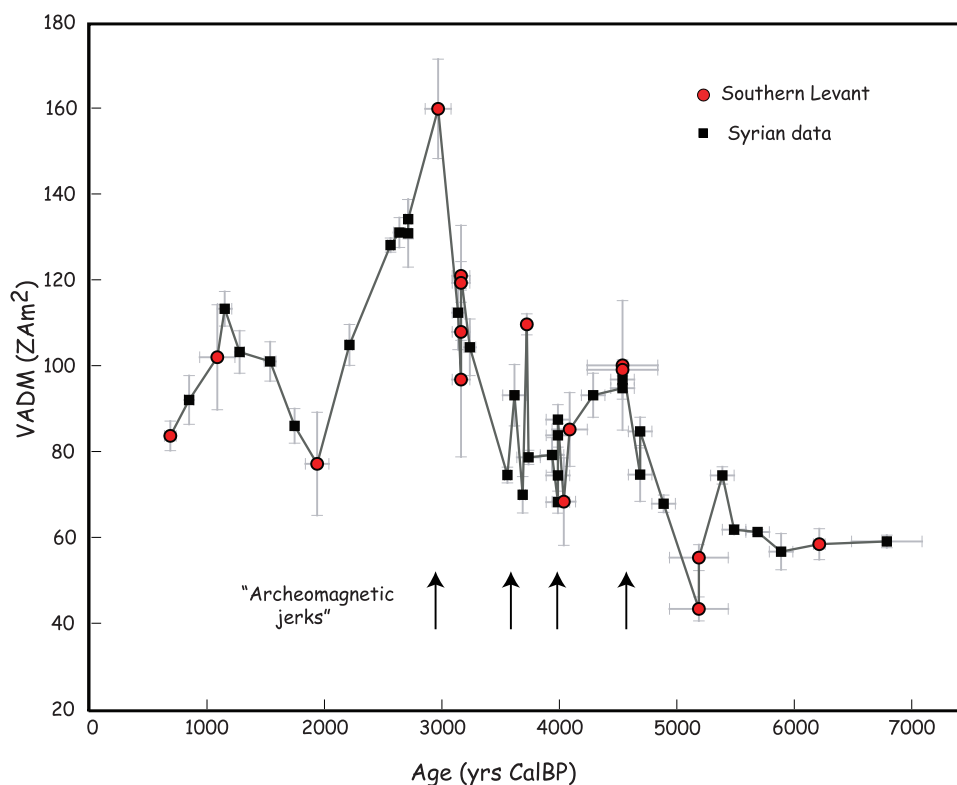
Figure 18. Curve combining Syrian [*Genevey et al.*, 2003; *Gallet and Le Goff*, 2006; *Gallet et al.*, 2006] and well dated Southern Levantine results meeting the 20% or 5 μT standard deviation cutoff (this study). Also shown are the "archeomagnetic jerks" of *Gallet et al.* [2006].

conspicuous peak in intensity around 3000 years ago (Iron Age) and there was a relatively long period of low intensity prior to 5000 years ago (Chalcolithic-Early Bronze Age). Two less prominent peaks are around 4500 years ago (Early Bronze Age II-3) and 1200 years ago (Early Islamic). Our data suggest an even higher peak than was previously published during the early Iron Age (ca 3100 years ago) and a slightly lower trough through in the Early Roman period (ca 2000 CalBP).

[78] Not surprisingly, the details of the archaeointensity curve do not agree well with the smoother depiction of the global model of *Korte and Constable* [2005a] (see Figure 16a). Nevertheless, most of the major trends of the geomagnetic intensity are reflected in the model. It seems to us that the reasons for the discrepancy are (1) the current low resolution of the global model and (2) the use of some less reliable data (e.g., that of *Games* [1980]) in constraining it. The published data include a variety of approaches, materials, and quality controls on paleointensity and dating, hence may contain a less than optimal recording of the geomagnetic field.

[79] *Gallet et al.* [2006] extended the observation that episodes of rapid change in the geomagnetic field intensity occurred several times over the last 5000 years, the so-called "archaeomagnetic jerks" of *Gallet et al.* [2003] (see Figure 18). Our new results (red dots) support the contention that there are at least four episodes of rapid increases in the geomagnetic field intensity, around 4600, 4000, 3600,

and 3000 years ago, although whether or not they are in fact "jerks" remains an open question.

[80] The occurrence of episodes of rapid change in the Earth magnetic field intensity, as well as the existence of a prominent peak around 3000 years ago should be further investigated. With the thick stacks of slag deposits which contains embedded charcoals, we see the great potential of this medium to contribute to the questions presented. Slag deposits can provide well dated and high resolution solutions, especially for those periods with rapid changes in the Earth magnetic field intensity.

11.4. Contribution to the Archaeological Research

[81] We obtained reliable archaeointensity results also from slag samples with either contested or poorly constrained dates (Figure 16b). These represent eight different archaeometallurgical sites from Israel and Jordan, some of which are in the center of archaeological debate regarding their dating (e.g., the site of Timna 39, *Avner* [2002]). Comparing these archaeointensity results with those from well dated slag samples and with the Syrian archaeointensity curve allows some interesting inferences about the archaeometallurgical picture of the region. For example, the data from IS11, the hotly debated site related to the dawn of copper production in the Timna region, suggest that this site may have been reoccupied many times over a 2000 year period. This comparative approach can be used also in future cases to give better age constraints for poorly

dated sites. The archaeological implications of our study, as well as the archaeological application of slag archaeointensity research will be discussed elsewhere.

12. Conclusions

[82] In this paper we have demonstrated the suitability of copper slag material in archaeointensity research. Using this medium together with a sophisticated experimental protocol (the "IZZI") we obtained consistent archaeointensity results from the last seven millennia. Our results show good agreement with the recently published data sets from Syria, and augment the existing record of the geomagnetic field intensity. Our data support trends in the field intensity changes, such as the relatively low prior to 5000 years ago and the conspicuous peak around 3000 years ago. They also support the existence of several short episodes of rapid change of the geomagnetic field intensity. The recently accumulated high quality data show that the global model [*Korte and Constable*, 2005a] underestimates the variability of the geomagnetic field.

[83] Slag material has further potential for archaeointensity research. Applying a preexperiment selection procedure may well increase the success rate, and using embedded charcoal for direct dating will increase the dating precision. In many localities, slag accumulated in multilayer mounds that can provide samples for high resolution investigation of specific periods of interest, such as the peak in the Iron Age or episodes of rapid intensity changes.

[84] Copper production sites can be found in many parts of the Old World, as well as certain locations in the New World, covering different and complementary time ranges since the invention of copper industry, approximately 7000 years ago. Using this material for archaeointensity reconstruction will open another door toward better understanding of the Earth's magnetic field in the late Holocene.

References

Adams, R. (1999), The development of copper metallurgy during the Early Bronze Age of the Southern Levant: evidence from the Faynan Region, Southern Jordan, Ph.D. thesis, Univ. of Sheffield, Sheffield, UK.

Aitken, M., P. Alcock, G. D. B., and C. Shaw (1981), Archaeomagnetic determination of the past geomagnetic intensity using ancient ceramics: Allowance for anisotropy, *Archaeometry*, 23, 53–64.

Aitken, M., A. Allsop, G. Bussell, and M. Winter (1984), Geomagnetic intensity in Egypt and western Asia during the second millennium BC, *Nature*, 310, 305–306.

Aitken, M. J., A. L. Allsop, G. D. Bussell, and M. B. Winter (1988), Determination of the intensity of the Earth's magnetic field during archaeological times: Reliability of the Thellier technique, *Rev. Geophys.*, 26, 3–12.

Athavale, R. (1969), Intensity of the geomagnetic field in pre-historic Egypt, *Earth Planet. Sci. Lett.*, 6, 221–224.

Avner, U. (2002), Studies in Material and Spiritual Culture of the Negev and Sinai Populations During 6th-3rd Millennia B.C., Ph.D. dissertation, Hebrew Univ. of Jerusalem, Jerusalem, Israel.

Avner, U., and J. Magness (1998), Early Islamic Settlement in the Southern Negev, *Bull. Am. Sch. Oriental Res.*, 310, 39–57.

Avner, U., and A. Naor (1978), A Survey in the Eilat Area, *Hadashot Arkheologiot*, pp. 66–68 (in Hebrew).

Bachmann, H. (1980), Early copper smelting techniques in Sinai and in the Negev as Deduced from Slag Investigations, in *Scientific Studies in Early Mining and Extractive Metallurgy*, edited by P. Craddock, *British Museum Occasional Paper*, pp.103–134, British Museum, London.

Bloxham, J. (2003), Dipole decay, secular variation and reversals, *Eos Trans. AGU*, 84(F34), Fall Meet. Supp. U42A-03.

Burakov, K., and I. Nachasova (1988), Measurement of the intensity of the geomagnetic field in the territory of Georgia during the 5th-3rd millenia BC, *Geomagn. Aeron.*, Engl. Transl., 28, 900–901.

Burleigh, R., and A. Hewson (1979), British museum natural radiocarbon measurements XI, *Radiocarbon*, 21, 339–352.

Burton, M., and T. Levy (2001), The chalcolithic radiocarbon record and its use in southern Levantine archaeology, in *Near East Chronology: Archeology and Environment*, edited by H. Bruins, I. Carmi, and E. Boaretto, *Radiocarbon*, 43, 1223–1246.

Coe, R. S. (1967), The determination of paleo-intensities of the Earth's magnetic field with emphasis on mechanisms which could cause non-ideal behavior in Thellier's method, *J. Geomagn. Geoelectr.*, 19, 157–178.

Coe, R. S., S. Grommé, and E. A. Mankinen (1978), Geomagnetic paleointensities from radiocarbon-dated lava flows on Hawaii and the question of the Pacific nondipole low, *J. Geophys. Res.*, 83, 1740–1756.

Folgheraiter, G. (1899), Sur les variations sèculaires de l'inclinaison magnètique dans l'antiquité, *J. Phys.*, 5, 660–667.

Gallet, Y., and M. Le Goff (2006), High-temperature archaeointensity measurements from Mesopotamia, *Earth Planet. Sci. Lett.*, 241, 159–173.

Gallet, Y., A. Genevey, and V. Courtillot (2003), On the possible occurrence of 'archaeomagnetic jerks' in the geomagnetic field over the past three millennia, *Earth Planet. Sci. Lett.*, 214, 237–242.

Gallet, Y., A. Genevey, M. Le Goff, F. Fluteau, and S. Ali Eshraghi (2006), Possible impact of the Earth's magnetic field on the history of ancient civilizations, *Earth Planet. Sci. Lett.*, 246, 17–26.

Games, K. P. (1980), The magnitude of the archaeomagnetic field in Egypt between 3000 and 0 BC, *Geophys. J. R. Astron. Soc.*, 63, 45–56.

Genevey, A., and Y. Gallet (2002), Intensity of the geomagnetic field in western Europe over the past 2000 years: New data from ancient French pottery, *J. Geophys. Res.*, 107(B11), 2285, doi:10.1029/2001JB000701.

Genevey, A., Y. Gallet, and J. Margueron (2003), Eight thousand years of geomagnetic field intensity variations in the eastern Mediterranean, *J. Geophys. Res.*, 108(B5), 2228, doi:10.1029/2001JB001612.

Gilead, I. (1994), The history of the chalcolithic settlement in the Nahal Beer Sheva Area: The Radiocarbon Aspect, *Bull. Am. Sch. Oriental Res.*, 296, 1–13.

Golani, A. (2004), Salvage excavations at the Early Bronze Age site of Ashqelon Afridar Area E, *'Atiqot*, 45, 9–62.

Gophna, R. (2004), Excavations at Ashqelon, Afridar - Introduction, *'Atiqot*, 45, 1–8.

Halgedahl, S., R. Day, and M. Fuller (1980), The effect of cooling rate on the intensity of weak-field TRM in single-domain magnetite, *J. Geophys. Res.*, 95, 3690–3698.

Hauptmann, A. (1989), The earliest periods of copper metallurgy in Fenan, Jordan, in *Old World Archaeometallurgy*, edited by A. Hauptmann, E. Pernicka, and G. Wager, pp. 119–135, Deutsche Bergbau-Museum, Bochum .

Hauptmann, A. (2000), *Zur frühen Metallurgie des Kupfers in Feinan/ Jordanien*, Der Anschnitt, Bochum.

Hauptmann, A., and G. Weisberger (1987), Archaeometallurgical and mining-archaeological investigations in the area of Feinan, Wadi Arabah (Jordan), *Annu. Dep. Antiquities Jordan*, 31, 419–435.

Hauptmann, A., and G. Weisberger (1992), Periods of ore exploitation and metal production in the area of Feinan, Wadi Arabah, Jordan, *Stud. Hist. Archaeol. Jordan*, 4, 61–66.

Hext, G. R. (1963), The estimation of second-order tensors, with related tests and designs, *Biometrika*, 50, 353–357.

Hulot, G., C. Eymin, B. Langlais, M. Mandea, and N. Olsen (2002), Small-scale structure of the geodynamo inferred from Oersted and Magsat satellite data, *Nature*, 416, 620–623.

Hussain, A. (1983), Archaeomagnetic investigations in Egypt: Inclination and field intensity determinations, *J. Geophys.*, 53, 131–140.

Hussain, A. (1987), The secular variation of the geomagnetic field in Egypt in the last 5000 years, *Pure Appl. Geophys.*, 125, 67–90.

Ilan, D. (1999), Northeastern Israel in the Iron Age I: Cultural, Socioeconomic and Political Perspectives, Ph.D. thesis, Tel-Aviv University, Tel Aviv, Israel.

Jackson, A., A. R. T. Jonkers, and M. R. Walker (2000), Four centuries of geomagnetic secular variation from historical records, *Philos. Trans. R. Soc. Ser. A*, 358, 957–990.

Kirschvink, J. L. (1980), The least-squares line and plane and the analysis of paleomagnetic data, *Geophys. J. R. Astron. Soc.*, 62, 699–718.

Korte, M., and C. Constable (2005a), Continuous geomagnetic field models for the past 7 millennia: 2. CALS7K, *Geochem. Geophys. Geosyst.*, *6*, Q02H16, doi:10.1029/2004GC000801.

Korte, M., and C. Constable (2005b), The geomagnetic dipole moment over the last 7000 years - New results from a global model, *Earth Planet. Sci. Lett.*, *236*, 348–358.

Korte, M., and C. G. Constable (2006), Centennial to millennial geomagnetic secular variation, *Geopys. J. Int.*, *167*, 43–52.

Korte, M., A. Genevey, C. Constable, U. Frank, and E. Schnepp (2005), Continuous geomagnetic field models for the past 7 millennia: 1. A new global data compilation, *Geochem. Geophys. Geosyst.*, *6*, Q02H15, doi:10.1029/2004GC000800.

Kovacheva, M., N. Jordanova, and V. Karloukovski (1998), Geomagnetic field variations as determined from Bulgarian archeomagnetic data. part II: The last 8000 years, *Surv. Geophys.*, *19*, 431–460.

Levy, T. (2006), Grand narratives, technological revolutions and the past: Deep-time studies of metallurgy and social evolution in the Eastern Mediterranean, in *Connectivity in Antiquity - Globalization as a Long-Term Historical Process, Approaches to Anthropological Archaeology*, edited by Ø. S. Labianca and S. A. Scham, pp. 10–25, Equinox, London.

Levy, T., and S. Shalev (1989), Prehistoric metalworking in the southern Levant: Archaeometallurgical and social perspectives, *World Archaeol.*, *20*, 272–352.

Levy, T., J. Anderson, M. Waggoner, N. Smith, A. Muniz, and R. Adams (2001), Digital archaeology 2001: GIS-based excavation recording in Jordan, *SAA Archaeol. Record*, *3*, 23–29.

Levy, T., R. Adams, A. Hauptmann, M. Prange, S. Schmitt-Strecker, and M. Najjar (2002), Early Bronze Age metallurgy: A newly discovered copper manufactory in southern Jordan, *Antiquity*, *76*, 425–427.

Levy, T., R. Adams, M. Najjar, M. Robinson, and T. Higham (2004), Reassessing the chronology of Biblical Edom: New excavations and ^{14}C dates from Khirbat en Nahas (Jordan), *Antiquity*, *78*, 863–876.

Levy, T., M. Najjar, J. van der Plicht, N. Smith, H. Bruins, and T. Higham (2005), Lowland Edom and the high and low chronologies: Edomite state formation, the Bible and recent archaelogical research in Southern Jordan, in *The Bible and Radiocarbon Dating: Archaeology Text and Science*, edited by T. E. Levy and T. Higham, pp. 129–163, Equinox, London.

Lupu, A. (1970), Metallurgical aspects of Chalcolithic copper working at Timna (Israel), *Bull. Hist. Metal. Group*, *4*, 21–23.

Lupu, A., and B. Rothenberg (1980), The extractive metallurgy of the Early Iron Age copper industry in the Arabah, Israel, *Archaeol. Austriaca*, *47*, 91–130.

Merkel, J. (1990), Experimental reconstruction of Bronze Age Copper smelting based on archaeological evidence from Timna, in *Researches in the Arabah 1959–1984*, vol. 2, *The Ancient Metallurgy of Copper*, edited by B. Rothenberg, pp. 78–122, Institute for Archaeo-Metal. Stud., London.

Meshel, Z. (1993), Yotvata Israel Exploration Society and Carta, in *The New Encyclopedia of Archaeological Excavations in the Holy Land*, edited by E. Stern, vol. IV, pp. 1517–1520, Yotvata Israel Exploration Society and Carta, Jerusalem.

Muhly, J. (1984), Timna and King Solomon, *Bibl. Orient.*, *XLI*, 276–292.

Nachasova, I., and K. Burakov (1995), Geomagnetic archaeointensity in the 5th millennium BC in Northern Mesopotamia, *Geomagn. Aeron.*, *35*, 131–137.

Nachasova, I., and K. Burakov (2000), The geomagnetic field intensity in Central Asia from 6000 to 3000 BC, *Izv. Phys. Solid Earth*, *36*, 358–363.

Nagata, T., Y. Arai, and K. Momose (1963), Secular variation of the geomagnetic total force during the last 5000 years, *J. Geophys. Res.*, *68*, 5277–5282.

Odah, H. (1999), Improvement of the secular variation curve of the geomagnetic field in Egypt during the last 6000 years, *Earth Planet. Phys.*, *51*, 13,225–13,229.

Odah, H., F. Heider, A. Hussain, V. Hoffmann, H. Soffel, and M. ElGamili (1995), Paleointensity of the geomagnetic field in Egypt from 4000 BC to 150 AD using the Thellier method, *J. Geomagn. Geoelectr.*, *47*, 41–58.

Peristykh, A., and P. Damon (2003), Persistence of the Glessberg 88-year solar cycle over the last 12,000 years: Evidence from cosmogenic isotopes, *J. Geophys. Res.*, *108*(A1), 1003, doi:10.1029/2002JA009390.

Rezlescu, N., and E. Cuciureanu (1970), Cation distribution and Curie temperature in some ferrites containing copper and manganese, *Phys. Stat. Solidi A*, *8*, 873–878.

Riisager, P., and J. Riisager (2001), Detecting multidomain magnetic grains in Thellier palaeointensity experiments, *Phys. Earth Planet. Inter.*, *125*, 111–117.

Rothenberg, B. (1978), Excavation at Timna Site 39, in *Chalcotithic Copper Smelting*, edited by B. Rothenberg, pp. 1–26, Institute for Archaeo-Metal. Stud., London.

Rothenberg, B. (1987), Pharaonic copper mines in southern Sinai, *Inst. Archaeo-Metal. Stud. Newsl.*, *10*, 1–7.

Rothenberg, B. (Ed.) (1990), *Researches in the Araba 1959–1984*, vol. 2, *The Ancient Metallurgy of Copper*, Inst. for Archaeo-Metal. Stud., London.

Rothenberg, B. (1999), Archaeo-metallurgical researches in the Southern Arabah 1959–1990. part I: Late pottery Neolthic to Early Bronze IV, *Palestine Explor. Q.*, *131*, 68–89.

Rothenberg, B., and J. Glass (1992), Beginnings and development of early metallurgy and the settlement and chronology of the Western Arabah, from the Chalcolithic Period to Early Bronze Age IV, *Levant*, *24*, 141–157.

Rothenberg, B., and C. Shaw (1990a), The Discovery of a Copper Mine and smelter from the end of the Early Bronze Age (EBIV) in the Timna Valley, *Inst. Archaeo-Metal. Stud. Newsl.*, *15–16*, 1–8.

Rothenberg, B., , and C. Shaw (Eds.) (1990b), *Chalcolithic and Early Bronze Age IV Copper Mining and Smelting in Timna Valley (Israel) - Excavations 1984–1990*, Ancient Mining and Metallurgy in Southern Europe, Belgrad.

Schabes, M. E., and H. N. Bertram (1988), Magnetization processes in ferromagnetic cubes, *J. Appl. Phys.*, *64*, 1347–1357.

Schlomovitz, N., M. Bar-Matthews, A. Segev, and A. Matthews (1999), Sedimentary and epigenetic copper mineral assemblage in the Cambrian Timna Formation, southern Israel, *Israel J. Earth Sci.*, *48*, 195–208.

Segal, D., and I. Carmi (1996), Rehovot Radiocarbon Date List V, *'Atiqot*, 79–106.

Segal, D., and I. Carmi (2004), Determination of age using the ^{14}C method on archaeobotanical samples from Ashqelon, Afridar Area E, *'Atiqot*, *45*, 119–120.

Segal, I., L. Halicz, and A. Kamenski (2004), The metallurgical remains from Ashqelon, Afridar Areas E, G and H, *'Atiqot*, *45*, 311–330.

Selkin, P., and L. Tauxe (2000), Long-term variations in paleointensity, *Philos. Trans. R. Astron. Soc.*, *358*, 1065–1088.

Selkin, P., J. Gee, L. Tauxe, W. Meurer, and A. Newell (2000), The effect of remanence anisotropy on paleointensity estimates: A case study from the Archean Stillwater complex, *Earth Planet. Sci. Lett.*, *182*, 403–416.

Selkin, P., J. S. Gee, and L. Tauxe (2007), Nonlinear thermoremanence acquisition and implications for paleointensity data, *Earth Planet. Sci. Lett.*, *256*, 81–89.

Shalev, S., and P. Northover (1987), The chalcolithic metal and metalworking from Shiqmim, in *Shiqmim I - Studies Concerning Chalcolithic Societies in the Northern Negev Desert, Israel (1982–1984)*, edited by T. Levy, pp. 357–371, Oxford.

Sharon, M., U. Avner, and D. Nahlieli (1996), An early Islamic mosque near Be'er Ora in the Southern Negev: Possible evidence for an early eastern Qiblah?, *'Atiqot*, *XXX*, 107–119.

Simmons, A. H. (2007), *The Neolithic Revolution in the Near East: Transforming the Human Landscape*, Univ. of Arizona Press, Tucson.

Tauxe, L., J. L. Steindorf, and A. J. Harris (2006), Depositional remanent magnetization: Toward an improved theoretical and experimental foundation, *Earth Planet. Sci. Lett.*, *244*, 515–529.

Tauxe, L., and H. Staudigel (2004), Strength of the geomagnetic field in the Cretaceous Normal Superchron: New data from submarine basaltic glass of the Troodos Ophiolite, *Geochem. Geophys. Geosyst.*, *5*, Q02H06, doi:10.1029/2003GC000635.

Tauxe, L., and T. Yamazaki (2007), Paleointensities, in *Treatise on Geophysics*, edited by M. Kono, *Treatise on Geophysics*, 5, 509–563, Elsevier, New York.

Tauxe, L., H. Bertram, and C. Seberino (2002), Physical interpretation of hysteresis loops: Micromagnetic modelling of fine particle magnetite, *Geochem. Geophys. Geosyst.*, *3*(10), 1055, doi:10.1029/2001GC000241.

Thellier, E. (1938), Sur l'aimantation des terres cuites et ses applications gèophysique, *Ann. Inst. Phys. Globe Univ. Paris*, *16*, 157–302.

Thellier, E., and O. Thellier (1959), Sur l'intensité du champ magnétique terrestre dans le passé historique et géologique, *Ann. Geophys.*, *15*, 285–378.

Usoskin, I., S. Solanki, and M. Korte (2006), Solar activity reconstructed over the last 7000 years: The influence of geomagnetic field changes, *Geophys. Res. Lett.*, *33*, L08103, doi:10.1029/2006GL025921.

Valet, J.-P. (2003), Time variations in geomagnetic intensity, *Rev. Geophys.*, *41*(1), 1004, doi:10.1029/2001RG000104.

Walton, D. (1977), Archeomagnetic intensity measurements using a SQUID magnetometer, *Archaeometry*, *19*, 192–200.

Walton, D. (1986), Alteration and its effects on the reproducibility of archaeomagnetudes from Tel El Amarana, *J. Geomagn. Geoelectr.*, *38*, 1349–1352.

Walton, D. (1990), Changes in the intensity of the geomagnetic field, *Geophys. Res. Lett.*, *17*, 2085–2088.

Watson, G. (1983), Large sample theory of the Langevin distributions, *J. Stat. Plann. Inference*, *8*, 245–256.

Willis, L. (1990), Exploring the ancient copper mines of the Wadi Amram (South Arabah), *Inst. Archaeo-Metall. Stud. Newsl.*, *15/16*, 12–15.

Yamazaki, T., and H. Oda (2002), Orbital influence on Earth's magnetic field: 100,000-year periodicity in inclination, *Science*, *295*, 2435–2438.

Yu, Y., L. Tauxe, and A. Genevey (2004), Toward an optimal geomagnetic field intensity determination technique, *Geochem. Geophys. Geosyst.*, *5*, Q02H07, doi:10.1029/2003GC000630.

————————————

A. Agnon and H. Ron, Institute of Earth Sciences, The Hebrew University of Jerusalem Givat Ram, Jerusalem, Israel, 91904. (amotz@cc.huji.ac.il; hagairon@vms. huji.ac.il)

U. Avner, The Arava Institute for Environmental Studies, Kibbutz Ketura, M. P. Hevel Eilot, 88840 Israel. (uzia@012.net.il)

E. Ben-Yosef, and T. E. Levy, Department of Anthropology, University of California, San Diego, Social Sciences Building 216, Mail Code 0532, 9500 Gilman Drive, La Jolla, CA 92093-0532, USA. (ebenyose@ucsd.edu; tlevy@ucsd.edu)

A. Genevey, Centre de Recherche et de Restauration des Musées de France, Palais du Louvre, Paris, France. (agnes.genevey@culture.gouv.fr)

M. Najjar, Department of Antiquity of Jordan, Amman, Jordan. (m.najjar@doa.jo)

L. Tauxe, Scripps Institution of Oceanography, University of California, San Diego, Mail Code 0220, La Jolla, CA 92093, USA. (ltauxe@ucsd.edu)